ACS APPLIED MATERIALS & INTERFACES

Subscriber access provided by UNIV OF NOTTINGHAM

Biological and Medical Applications of Materials and Interfaces

Polymer microparticles with defined surface chemistry and topography mediate the formation of stem cell aggregates and cardiomyocyte function

Marta Alvarez-Paino, Mahetab H Amer, Aishah Nasir, Valentina Cuzzucoli Crucitti, David Needham, Chris Denning, Morgan R. Alexander, Felicity Rose, and Cameron Alexander

ACS Appl. Mater. Interfaces, **Just Accepted Manuscript** • DOI: 10.1021/acsami.9b04769 • Publication Date (Web): 20 Jun 2019

Polymer Microparticles with Defined Surface Chemistry and Topography Mediate the Formation of Stem Cell Aggregates and Cardiomyocyte Function

Marta Alvarez-Paino[1‡], Mahetab H. Amer[1‡], Aishah Nasir[2], Valentina Cuzzucoli Crucitti,[3] David Needham,[1] Chris Denning[2], Morgan R. Alexander[1], Felicity R. A. J. Rose[1*] and Cameron Alexander.[1*]

1. School of Pharmacy, University of Nottingham, Nottingham, NG7 2RD, UK.

2. Department of Stem Cell Biology, Faculty of Medicine & Health Sciences, University of Nottingham, Nottingham, NG7 2RD, UK.

3. Department of Chemical and Environmental Engineering, Faculty of Engineering, University of Nottingham, Nottingham, NG7 2RD, UK.

‡These authors contributed equally to the work

Keywords: Cell-material interfaces, cardiomyocyte function, mesenchymal stem cells, polymer microparticles, surface-initiated polymerization, surface topography.

Abstract: Surface-functionalized microparticles are relevant to fields spanning engineering and biomedicine, with uses ranging from cell culture to advanced cell delivery. Varying topographies of biomaterial surfaces are also being investigated as mediators of cell-material

interactions and subsequent cell fate. To investigate competing or synergistic effects of chemistry and topography in three-dimensional (3D) cell cultures, methods are required to introduce these onto microparticles without modification of their underlying morphology or bulk properties. In this study, a new approach for surface functionalization of poly(lactic acid) (PLA) microparticles is reported that allows decoration of the outer shell of the polyesters with additional polymers via aqueous atom transfer radical polymerization (ATRP) routes. PLA microparticles with smooth or dimpled surfaces were functionalized with poly(poly(ethylene glycol) methacrylate) (pPEGMA) and poly[N-(3-aminopropyl)methacrylamide] (pAPMA) brushes, chosen for their potential abilities to mediate cell adhesion. X-ray Photoelectron Spectroscopy (XPS) and Time-of-Flight Secondary Ion Mass Spectrometry (ToF-SIMS) analysis indicated homogeneous coverage of the microparticles with polymer brushes while maintaining the original topographies. These materials were used to investigate the relative importance of surface chemistry and topography both on the formation of human immortalized mesenchymal stem cell (hiMSCs) particle-cell aggregates and on the enhanced contractility of cardiomyocytes derived from human induced pluripotent stem cells (hiPSC-CMs). The influence of surface chemistry was found to be more important on the size of particle-cell aggregates than topographies. In addition, surface chemistries that best promoted hiMSC attachment also improved hiPSC-CM attachment and contractility. These studies demonstrated a new route to obtain topo-chemical combinations on polyester-based biomaterials, and provided clear evidence for the predominant effect of surface functionality over micron-scale dimpled topography in cell-microparticle interactions. These findings thus provide new guiding principles for the design of biomaterial interfaces to direct cell function.

Introduction

Hydrolytically degradable polyesters, such as poly(lactic acid) (PLA), poly(glycolic acid) (PGA), their co-polymer poly(lactic-co-glycolic acid) (PLGA) and polycaprolactone (PCL), are widely used in many biomaterials applications.[1-3] These polyesters have good biocompatibility, exhibit good mechanical properties, and their degradation profiles can be tuned via alteration in co-monomer content according to the clinical application required. Of most importance to date has been the use of PLA and PLGA implants and microparticles for drug delivery, where the polymer acts as a solid reservoir, degrading over time to release drugs, peptide hormone-mimetics and growth factors.[4] The low chemical reactivity of PLA is advantageous when the polymer is used as a solid matrix for encapsulating biological therapeutics, but limiting when there is a need to control the interaction of PLA with cells or tissue. This is because the surface of bulk PLA is relatively hydrophobic and adsorbs proteins and other amphiphiles indiscriminately from biological environments, unless modified with appropriate surface functionality.[5-6]

Accordingly, there have been a number of methods developed to derivatize PLA surfaces to enhance or control their interactions with biomolecules and cells.[7] These include plasma treatment,[8] solvent swelling followed by polymer entrapment from solvent/non-solvent mixtures,[9] and adsorption or grafting of amphiphilic co-polymers.[10-12] In many cases, the aim has been to promote attachment of eukaryotic cells so that the PLA matrix can act as a support for tissue growth, and multiple papers have shown that chemical functionalization of the biomaterial's surface can enhance or reduce the interactions between varying cell types and substrates.[13-17]

In addition to surface functionality, topography of biomaterial surfaces is known to play a role in modulating a number of cellular responses.[18-24] Biomaterials with surface features such as grooves, pits, columns, etc. have been shown to alter cell adhesion, mobility and morphology.[25-27] Furthermore, the spatial distribution and dimensions of topographical features also determine the way cells interact with

solid substrates.[28-29] Accordingly, there is a strong need to modulate both chemistry and topography on biomaterial surfaces to control cell-material interactions. [30-31]

In this work, we aimed to develop practical and robust methodologies to allow the modification of surface functionality at PLA surfaces while retaining the underlying morphology. We were particularly interested in methods allowing introduction of diverse chemistries to the surface of PLA microparticles of diameters in the 5-100 μm range, and with surface asperities of ~ 1-5 μm. Therefore, plasma treatments and solvent swelling methods were considered unsuitable, as these would not functionalize spherical microparticles evenly nor retain morphologies of the underlying materials after the swelling process. Therefore, we decided to grow functional polymer brushes from the surfaces, as established 'grafting from' techniques offer higher polymer densities and better control of the coating thickness compared to other methods.[32]

Previous reports have shown that polyester surfaces can be readily derivatized with amines (aminolysis) [33] under basic conditions, and thus we considered aminolysis as a versatile way to transform the "non-functional" surfaces of PLA into a substrate with convenient amine 'handles' for further modification. We therefore functionalized PLA-based microparticles in a stepwise manner with chemistries that retained the bulk properties of biodegradability while preserving the underlying microparticle topographies. The method involved the following three steps - (1) microparticle (MP) surface activation via aminolysis, (2) introduction of ATRP initiator groups via amidation, and (3) graft polymer formation via surface-initiated ARGET ATRP. This method was designed to be adaptable to the polymerization of a large variety of monomers, thus offering routes to production of polyester microparticles decorated with any polymer accessible via aqueous ATRP.

To exemplify this approach, we demonstrated the polymerization of the monomers 3-aminopropylmethacrylamide (APMA) and poly(ethyleneglycol)methacrylate (PEGMA) from PLA microparticles of two different topographies. These polymers were chosen because polyPEGMA has

shown good anti-fouling properties, owing to its ability to resist protein and cell attachment via steric and lone pair donor function[34-36] while pAPMA as a polycation was expected to promote eukaryotic cell attachment via a simple charge-charge interaction with proteins and the polyanionic cell membranes. In addition, we evaluated the untreated PLA microparticles, which carry surface negative charges in aqueous suspensions owing to ionization of carboxyl end-groups, and the aminolyzed PLA microparticles, which were expected to display positively charged surfaces from their 2-aminoethyl termini.

These methodologies enabled the production of microparticle surfaces with varying chemistries (aminolyzed, pPEGMA and pAPMA) and topographical features (smooth and dimpled) that could be varied independently. These materials were then evaluated to examine the relative importance of surface chemistry and topography on human immortalized mesenchymal stem cells (hiMSCs) attachment and formation of three-dimensional (3D) microparticle aggregates in co-culture. Selected microparticles from the above set were chosen to explore the effect of surface chemistry on attachment and contractility of cardiomyocytes derived from human induced pluripotent stem cells (hiPSC-CMs). These studies were used together to evaluate the effects of surface chemistry and topography of PLA microparticles for their use to support stem cell viability and cardiomyocyte function in 3D culture systems.

Experimental section

Materials

Poly(D,L-lactic acid) (PLA) (Evonik, Mn 47000 $gmol^{-1}$, IV~ 0.5 dL g^{-1}), fusidic acid (98%, Acros Organics), dichloromethane (DCM) (≥99.8, Fisher Scientific), poly(vinyl acetate-co-alcohol) (PVA) (MW 13-23 kDa, 98% hydrolysed, Sigma-Aldrich), ethylenediamine (Sigma-Aldrich), isopropanol (IPA) (≥99.9%, Fisher Scientific), 2,4,6-trinitrobenzenesulfonic acid solution (1M in H_2O, Sigma-Aldrich), sodium tetraborate (99%, Sigma-Aldrich), dimethyl sulfoxide (DMSO) (Thermo Scientific), α-

bromoisobutyryl bromide (BiBB, 98%, Sigma-Aldrich), hexane (Fisher Scietific), methanol (Fisher Scientific), poly(ethylene glycol) methacrylate (pPEGMA500) (Mn 500 g mol-1, Sigma-Aldrich), N-(3-Aminopropyl) methacrylamide hydrochloride (APMA) (98%, Sigma-Aldrich), phosphate buffered saline (PBS) (0.1M, pH 7.4, 0.15M NaCl), triethylamine (TEA) (99%, Sigma-Aldrich) and hexylamine (99%, Sigma-Aldrich). All other reagents were used as received.

Methods

Smooth and textured microparticle fabrication –

Smooth poly(D,L-lactic acid) (PLA) microparticles (MPs) were prepared by a solvent evaporation oil-in-water emulsion technique. The organic phase, containing 1 g of PLA in 5 mL of dichloromethane (DCM) (20% w/v) was homogenized (Silverson Homogenizer L5M) at 2000 rpm for 5 minutes in the aqueous continuous phase (100 mL) containing 1% w/v of poly(vinyl acetate-co-alcohol) (PVA) as stabilizer. The resulting emulsion was stirred continuously at 500 rpm at room temperature for at least 4 hours to allow for solvent evaporation. To remove residual PVA, microparticles were centrifuged at 4500 rpm for 5 min and subsequently washed with deionised (DI) water three times. Cell strainers with a pore size of 40 and 100 μm were used to separate microparticles in this size range and the collected microparticles were freeze-dried for storage at -20^{o}C.

To produce textured microparticles, fusidic acid (FA) was incorporated in the organic phase, as previously described[37] at 30% w/w to polymer (FA/PLA total content 10% w/v in DCM). The dispersed phase was then stirred at 600 rpm into the PVA aqueous solution (1% w/v). After solvent evaporation, microparticles were washed and collected. Dimpled microparticles were obtained after FA release under dynamic conditions in phosphate buffered saline (PBS) at 37°C over 7 days.

Surface activation via aminolysis

Smooth and dimpled PLA microparticles were placed in a plastic tube and 1 mL of 0.5M ethylenediamine (EDA) solution was added per each 10 mg of MPs. Treatment was performed at room temperature and microparticles were maintained continuously in motion with the aid of a roller shaker.

To investigate the effect of treatment conditions on the microparticle activation, aminolysis was carried out either in isopropanol (IPA) or borate buffer (BB) (0.1 M, pH~9) over different time periods. The microparticles were intensively washed with DI water (over 10 washing steps) after reaction with EDA until the reagent was completely removed from the supernatant (as confirmed by a with the 2,4,6-trinitrobenzenesulfonic acid (TNBS) colorimetric assay). During the washing procedure, the microparticles suspensions were maintained under continuous shaking in order to avoid any aggregation in the event of settling. The microparticles were separated from the supernatant via centrifugation at 1000 rpm for 2 mins, with careful monitoring again to avoidf aggregation). The amine-functionalized microparticles were finally collected by a further gentle centrifugation step, freeze dried and stored in the freezer (-20^{o}C) until further use.

ATRP initiator immobilisation

Aminolysed microparticles were re-suspended in 10 mL of hexane in a plastic tube and 1 mmol of triethylamine (140 μL) was added. The tube was then placed in an ice bath and the ATRP initiator precursor BiBB was added dropwise under gentle stirring. The reaction was maintained at 0°C for 2 hours and for an additional 4 hours at room temperature. After reaction, excess reagent was removed by centrifugation of the particle suspension at 3000 rpm for 3 min and washing with hexane four times. Bromoisobutyramide-functionalized microparticles were allowed to dry overnight at room temperature, prior to washing with DI water to remove the precipitated salts. The resultant microparticles were collected by centrifugation and freeze-drying.

Assessment of surface modification: TNBS assay

Primary amines at the microparticle surfaces were quantified with the 2, 4, 6-trinitrobenzenesulfonic acid (TNBS) colorimetric assay. Pre-washed MPs were re-suspended and gently shaken in 600 μL of borate buffer. After centrifugation, 485 μL of supernatant was collected and transferred to an Eppendorf tube. Then, 15 μL of TNBS reagent (1:30 diluted from a 1M solution with borate buffer) were added and the sample was incubated at room temperature in the dark for 30 min. Absorbance was measured at 420 nm (TECAN Infinite M200 microplate reader) and residual EDA was calculated from a calibration curve prepared with hexylamine in borate buffer in the concentration range 0.001-0.08 mM. Absorbance of the TNBS reagent was subtracted from all the measurements.

To determine the amount of accessible reactive amine groups on the MPs, functionalized microparticles (2.5 mg) were dissolved in 485 μL of DMSO. To each sample, 15 μL of TNBS reagent (prepared as above) were added and samples were incubated at room temperature in the dark. After 30 min, 200 μL from each sample were transferred in duplicate to a 96-well plate and absorbance was measured at 420 nm. The amine contents in each sample were determined from a calibration curve prepared with hexylamine in DMSO in the concentration range 0.001-0.08 mM (standards of hexylamine were freshly prepared and analyzed in parallel with the samples). Absorbances of untreated microparticles (2.5 mg) and TNBS reagent were also measured as controls and used to correct absorbance values of the samples and the calibration respectively.

Surface-initiated polymerization from microparticles

Grafting of poly(ethylene glycol) methacrylate (PEGMA) and N-(3-aminopropyl) methacrylamide (APMA) monomers was accomplished via surface-initiated activator regenerated by electron transfer - atom transfer radical (ARGET ATRP) from bromoisobutyramide-functionalized microparticles. Similar conditions to those reported previously were followed with slight modifications.[38] Polymerizations were performed at room temperature and at [monomer]:[catalyst]:[ligand]:[reducing

agent] molar ratio of 100 : 0.005 : 0.025 : 0.4. PEGMA polymerization was carried out in a mixture of 50/50 methanol/water while APMA was polymerized in 100% water.

pPEGMA grafting from microparticles

In a plastic bijou vial provided with a small magnetic stirrer and a rubber septum, bromoisobutyramide-(BIB)-functionalized microparticles (~200 mg) were re-suspended in 1 mL of DI water and degassed with N_2 for at least 20 min. In a separate glass tube, 0.5 g of PEGMA500 were dissolved in 2.25 mL of methanol and 1.25 mL of DI water (10% w/v monomer content in the final reaction mixture). Tris(2-pyridylmethyl)-amine (TPMA); 14.52 μL from a 5 mg mL^{-1} stock solution) and $CuBr_2$ (11.17 μL from a 1 mg mL^{-1}stock solution) were subsequently added to the solution and the mixture was degassed with N_2 for 15 min. Ascorbic acid (28.18 μL from a 25 mg mL^{-1} stock solution) was also added to the mixture which was degassed for further 10 min.

APMA grafting from microparticles

In a similar manner to PEGMA polymerization, BIB-functionalized microparticles were placed in a plastic bijou vial, re-suspended in 500 μL of DI water and degassed with N_2. TPMA (16.25 μL from 5 mg mL^{-1} solution) and $CuBr_2$ (12.50 μL from 1 mg mL^{-1} solution) were separately mixed in 100 μL of DI water and then added to the APMA solution previously prepared by dissolving 200 mg of the monomer in 370 μL of DI water. The mixture was degassed with N_2 for 15 min and then ascorbic acid (28.18 μL from 25 mg mL^{-1}solution) was also added to the mixture which was degassed for a further 10 min.

Polymerization reactions started immediately after addition of the corresponding reaction mixtures onto the microparticle suspensions. Stirring speed was maintained at 200 rpm to retain MP morphology. After 4 hours, polymerizations were stopped by exposure to air and microparticles were intensively washed with 50/50 methanol/water mixtures in the case of the pPEGMA-grafted MPs and

water only in the pAPMA-grafted MPs. In addition, control polymerizations in the absence of catalyst were also carried out to probe the efficacy of the surface-initiated ATRP from the microparticle surfaces.

Characterization

Microparticle size and size distribution analysis

Mean particle size and particle size distributions for both smooth and dimpled microparticles were measured using a Coulter LS230, laser diffraction particle size analyser (Beckman, UK). For the measurements, MPs were suspended in DI water and further DI water was added to the sample cell until 8-12% obscuration levels were reached. Microsphere size distribution was determined as a function of the microsphere diffraction and plotted as a function of volume percentage. Mean particle size and span values were obtained from the software statistics. For the textured microparticles, dimple size distribution was manually measured using Image J software. To ensure representative measurements, more than two hundred dimples were measured from three separate SEM images (collected as described below) and from at least 10 different microparticles.

Microparticle morphology characterization

Microparticles were imaged using a Jeol 6060LV Scanning Electron Microscopy (SEM). Samples were prepared from dispersions of microparticles in water, which were dropped onto aluminium stubs and gold-coated prior to scanning. SEM images were acquired at 10 kV acceleration voltage.

Surface characterization of functionalized microparticles

Time-of-flight secondary ion mass spectrometry (ToF-SIMS) measurements of the microparticles were conducted using an IONTOF ToF-SIMS IV instrument operated using a 25 keV Bi^{3+} primary ion source. Both positive and negative secondary ion spectra were collected over an acquisition period of 15 scans within the static acquisition regime (total ion dose $<1 \times 10^{12}$ ions cm^{-2}) and charge compensation was applied due to the non-conductive nature of the samples. For imaging, patch areas of 0.5×0.5 mm

were acquired at a resolution of 256 × 256 pixels. Data processing was carried out using SurfaceLab 6 software package.

X-ray photoelectron spectroscopy (XPS) analysis of the microparticles was performed on a Kratos Axis Ultra DLD equipped with a monochromated Al Kα X-ray source (hν = 1486.6 eV) operating at 10 kV and 15 mA (150 W). For data acquisition, survey spectra between 0-1000 eV binding energy (pass energy of 160 eV and 0.8 eV step size) and high resolution C 1s, O 1s, N 1s and Br 3d spectra were recorded using relative sensitivity factors provided by the manufacturer for quantification. All data was processed using CasaXPS software and charge referencing was made by reference to the C 1s hydrocarbon peak at 285.0 eV.

hiMSC - microparticle assays

The microparticles were weighed (3 mg), re-suspended in 100 µL PBS and transferred to CellStar® cell-repellent well plates (Greiner BioOne, UK). Assays were carried out with microparticles from 3 independent batches in triplicate. Immortalized human mesenchymal stem cells[39] were seeded onto the microparticles (6,000 cells/well for viability studies, 1500 cells/well for proliferation studies and 100,000 cells/well for aggregation studies) and cultured at 37°C, with 5% CO_2 in air.

Cell viability and aggregation studies: Assessment of viability was carried out using the LIVE/DEAD Viability/Cytotoxicity Kit for mammalian cells (ThermoFisher Scientific, UK) 48 hours post-seeding. Calcein AM and ethidium homodimer-1 were prepared in PBS to produce Live/Dead staining solution. Live cells stained green (calcein AM) and nuclei of dead cells stained red (ethidium homodimer-1). Samples were visualised using a Leica DR IRBE microscope, equipped with an automated stage and an attached Leica DC200 digital camera (Leica Microsystems Ltd., UK). Quantitation from images of Live/Dead-stained cells on untreated and functionalized microparticles, 6 hours post-seeding, was carried out using CellProfiler software (Broad Institute).[40] Five separate fields of view were randomly obtained from each well (n=3 microparticle batches) of a 24-well plate. Metrics

related to the number and size of aggregates were measured using the "Measure Object Size Shape" module.

Cell proliferation: PrestoBlue (ThermoFisher Scientific, UK) was used to determine cell proliferation by assessing cell numbers at days 1, 6 and 10. A mixture of PrestoBlue and culture medium (1:9) was added to each well and incubated in the dark at 37°C for 1 hour. Triplicate 100 µL aliquots were measured for fluorescence on a Tecan Infinite M200 microplate reader, using excitation and emission wavelengths of 560 and 590 nm, respectively.

hiPSC-CMs – microparticle assays

The hiPSC cell line, ReBl-PAT (referred to RPAT hereafter), was derived, cultured and differentiated as previously described.[41]

Untreated and three chemically modified smooth microparticles were weighed (0.75mg/well) and transferred to a 96-well microplate (Thermo Scientific Nunc, 167008) by resuspending in PBS. Microparticles were then washed three times in PBS, UV-sterilised (for 30 minutes) and incubated in medium (RPMI 1640 basal medium (Gibco #21875034) with B27 supplement (LifeTechnologies #0080085-SA), 10µM Y-27632 (ROCKi, Tocris Bioscience #0080085-SA) and 1% Penicillin-Streptomycin (P0781 Sigma-Aldrich) for at least 1 hour prior to seeding. RPAT-CMs were dissociated using a Collagenase II-based protocol as previously described[41] and seeded on microparticles (at days 13-16 for studies and days 22-25 after initiation of differentiation for contractility and aggregation studies respectively) at a seeding density of $4x10^5$ cells/well. Seeded microplates were immediately placed on an orbital rotary shaker (IKA KS 130 Basic; at 37°C, 5% CO_2 in air) for 15 minutes for aggregation studies and 30 minutes to form larger cell-microparticle aggregates for contractility studies. All experiments were subsequently carried out under static conditions for the remainder of the culture time.

Aggregation studies: Quantitation of contractile cell-microparticle aggregates (contraction used as a qualitative measure of cell viability) was derived from brightfield images (Operetta high content

imaging system, Perkin Elmer) taken 24hrs post-seeding. Images of nine separate fields were obtained for each well (n=3), from 2 independent batches of RPAT-CMs. Images were analysed using Harmony high-content image analysis software (Perkin Elmer) developed with PhenoLOGIC machine learning algorithms to quantify numbers of mean areas of cell-microparticle aggregates.

Contractility studies: Cell-microparticle aggregate cell motion was recorded 48 hrs post-seeding using high-speed video imaging (Camera FV-5 application attached to light microscope) and the CellOPTIQ platform (Clyde Biosciences Ltd, Glasgow, Scotland). Contractility measurements were analysed using MUSCLEMOTION[42] (open-source software). Contraction peaks that showed poor linearity (according to MUSCLEMOTION user manual) were excluded from analysis. Video images were selected from separate fields with high cell-microparticle interactions (untreated (n=20), aminolysed (n=23), PEGMA (n=41) and APMA (n=11)) for each well (untreated (n=6), aminolysed (n=6), PEGMA (n=9) and APMA (n=3), from 2 independent batches of RPAT-CMs.

Statistical analysis

Statistical data analysis (as stated in text) was performed using GraphPad Prism 7 software (GraphPad Software, CA, USA), with statistical outliers identified and excluded using robust regression and outlier remover (ROUT) analysis[43] with Q = 1%.

Results and discussion

Microparticles (MPs) of poly(D,L-lactic acid) were fabricated by the single oil-in-water solvent evaporation emulsion technique (Scheme 1).

Scheme 1. Preparation of surface-modified polymer microparticles. In (A), PLGA was dissolved in dichloromethane with, or without, fusidic acid (FA) and added with stirring into an aqueous phase containing PVA surfactant. After solvent evaporation, microparticles were obtained (B), which for the

FA-modified materials were washed in phosphate buffer to remove the additive and leave 'dimpled' particles (C). For surface grafting reactions particles (D) were reacted with ethylendiamine to form amine-functional microparticles (E). The surfaces were then reacted with 2-bromoisobutyrylbromide to form initiator-modified PLGA (F) enabling ATRP chemistries to generate polymer-grafted PLGA (G).

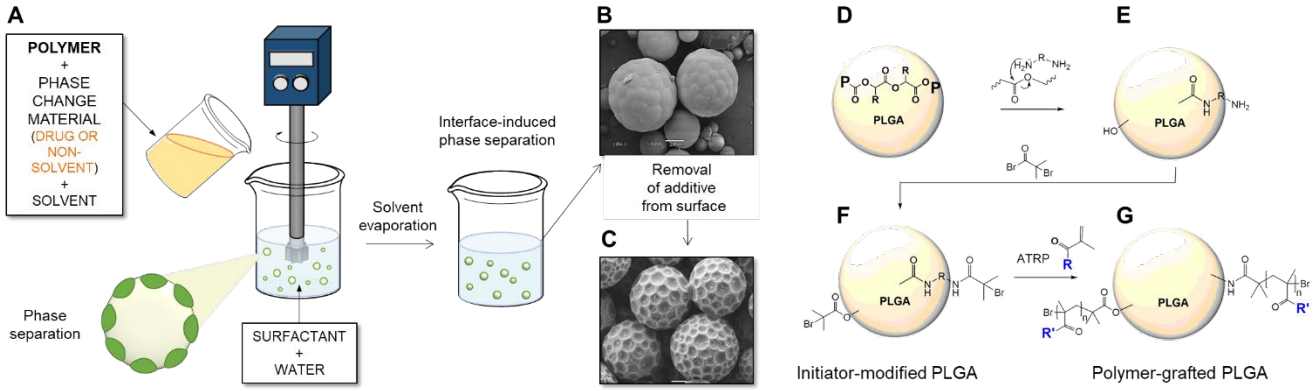

To achieve particles with the desired size, emulsion settings such as speed rate, polymer concentration, oil-to-water ratio, etc. were optimized. Under the indicated conditions (see methods section) and without the addition of any other component, smooth microparticles with a mean particle size of 60 ± 14 µm were obtained after filtration (Figure 1A). For the dimpled microparticles, a surface-layer phase separation process was induced by the addition of FA into the organic phase.[25] Due to the incompatibility of the FA and the PLA, the FA and polymer phase separated as the solvent evaporated during the emulsion process. At select FA/PLA ratios, FA-rich domains appeared homogeneously distributed across the surface of the MPs (Figure 1B). In the last step, removal of FA via washing revealed the topography of PLA MPs exhibiting a characteristic a dimpled pattern on their surface, sometime referred to as golf ball-like (Figure 1C). Dimpled MPs showed mean particle and dimple sizes of 64 ± 15 µm and 4 ± 1 µm respectively. The variation in size range values for both smooth and dimpled microparticles was reduced by up to 0.5 (20 CV%) after filtration.

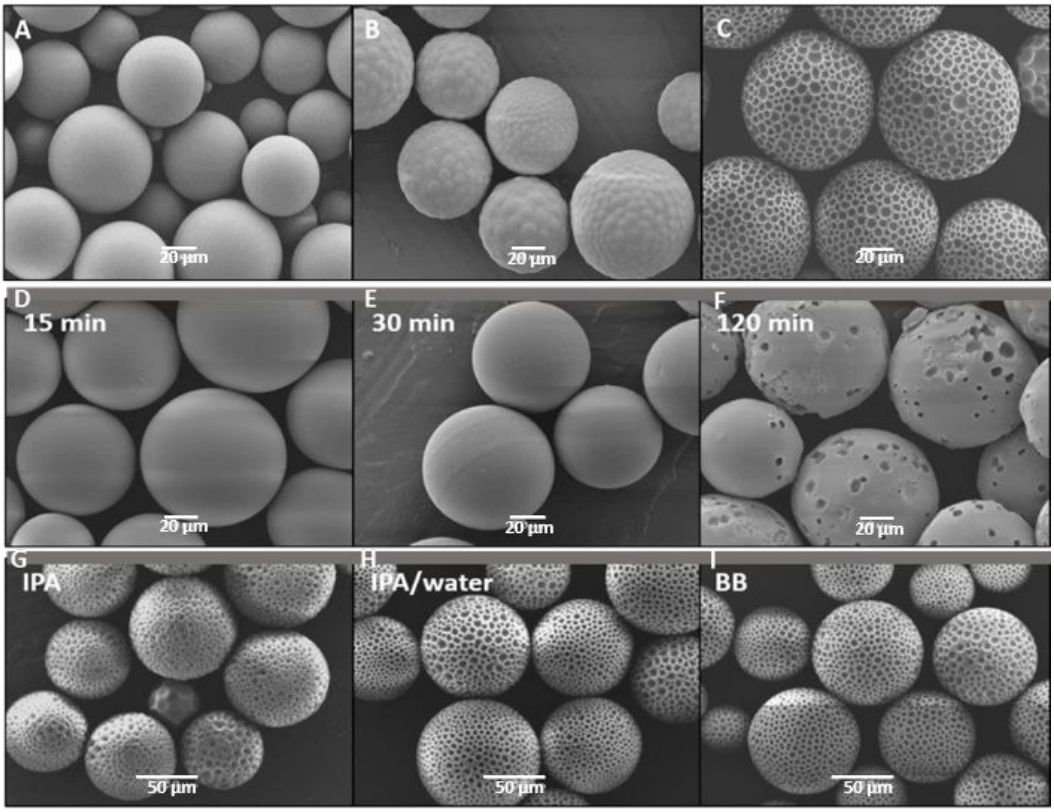

Figure 1. SEM micrographs of microparticles fabricated by oil-in-water emulsion technique. Smooth (A) and dimpled microparticles before (B) and after (C) FA release. In D-I, the effects of aminolysis with EDA 0.5M on microparticle morphology are presented as a function of time (D-F; IPA as solvent) and as a function of solvent (G-I; 20 mins treatment). Scale bars in SEM images A-F= 20µm, G-I = 50µm.

After microparticle fabrication, a 3-step approach for the functionalization of the PLA surfaces was developed. In this process, we used ethylenediamine (EDA) to cleave the ester bonds situated at the outermost layer of the surface and thus generate a new amide bond as well as free amino and hydroxyl groups. Reaction conditions were carefully controlled in order to modulate the aminolysis rate. We therefore investigated the influence of solvents, type of aminolysing agents, concentrations, temperatures and times on the reaction kinetics, as previously described for analogous chemistries.[12, 44] The TNBS

assay proved to be a suitable method for the rapid quantification of amines immobilized on the microparticles.[45-46] As shown in Figure 2, an increase in the exposure time resulted in a proportional increase in the amine content during the first 60 min of the reaction. However, continued treatment for a further 60 min did not result in greater modification, reaching a plateau above this point (figure 2B). In addition, microparticles exposed for periods no longer than 30 min maintained a well-conserved morphology but longer treatments were detrimental for the microparticle topographies (Figure 1 D-F). Therefore, a treatment of 20 min was found to be enough to achieve a good activation of the microparticles surface without compromising gross morphology. To test if these conditions were also valid for particles with modified topography, the same treatment was applied to dimpled microparticles. Even though isopropanol is a non-solvent for PLA, the dimpled texture was irreversibly affected during the treatment as a partial swelling of the microparticles was observed even after the shortest treatment of 5 min. To overcome this issue, mixtures of 50/50 IPA/water and borate buffer (pH 9.5) were also investigated as the reaction media. Basic aqueous conditions rather than neutral pH were employed, as the aminolysis process is favoured against hydrolysis when the pH is close to the pKa of the amine.[44] Under these conditions, the microparticles maintained the integrity of the dimpled features (Figure 1 G-I). However, amine quantification of the sample treated in IPA/water mixture showed a reduction of amino groups when compared to those obtained under IPA alone for equal treatment time (Figure 2A). Furthermore, microparticles treated in borate buffer for 20 min showed very little or no modification and as a consequence, the reaction time was increased up to 4 hours to generate substantial activation (Figure 2A). These findings were not unexpected as it is known that reaction rate greatly depends on the solvent chosen.[44] In addition, dimpled microparticles displayed more reactive amine groups than smooth microparticles due most likely to their larger surface areas.

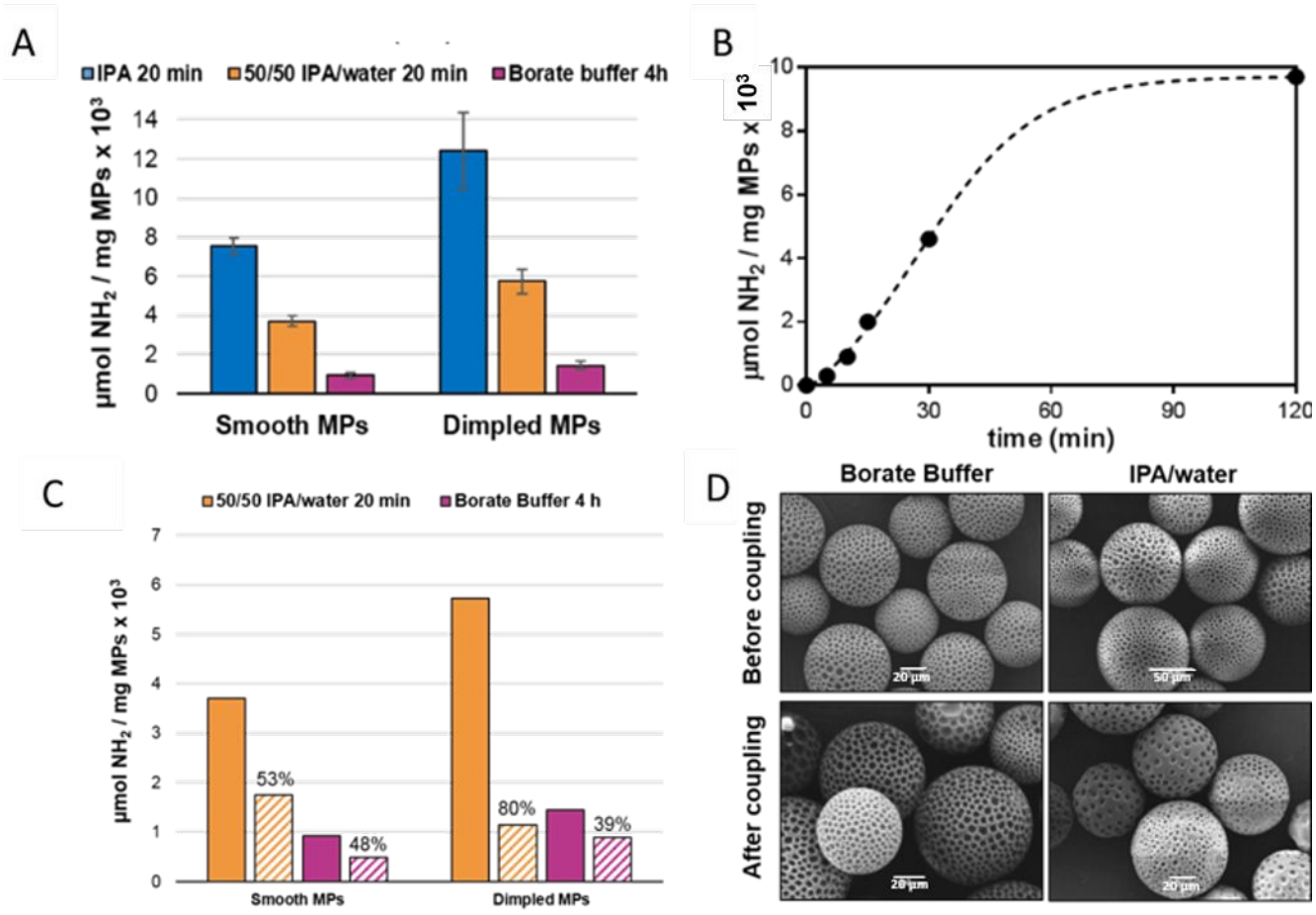

Figure 2. (A) Amine content after aminolysis of smooth and dimpled microparticles as a function of the solvent. (B) Amine content after aminolysis of smooth micropaticles with EDA 0.5M in IPA as a function of the treatment time. (C) Amine content on the MPs after aminolysis (filled bars) and after coupling reaction of BiBB (dashed bars). Numbers denote percentage of reduction of amine groups during this process. (D) SEM micrographs showing comparison of microparticle morphology before and after BiBB immobilization.

In the second step, BiBB was reacted with the hydroxyl and amino groups at the microparticle surface, and the TNBS assay was used to measure the extent of this reaction by means of the reduction in amine content of the samples. As can be seen in Figure 2C, a clear reduction in the amine content confirmed the success of the initiator immobilisation on the amine-functionalized microparticles. After 6 hours reaction, microparticles that were aminolysed in IPA/water mixtures reduced in amine content

by 53% and 80% for smooth and dimpled microparticles respectively, and by 48% and 39% for microparticles aminolysed in borate buffer. As shown by these values, complete coupling was not achieved despite the fact that a large excess of BiBB reagent was used and no further improvement in surface amidation was obtained after longer reaction times. It is likely that the bulky bromoisobutyryl functional groups encountered significant steric hindrance at the surface beyond a certain local concentration, preventing access of any further acyl bromides to the underlying amine functionality. Microparticles previously treated in IPA/water were more distorted after the coupling reaction compared to those treated in borate buffer, as shown in Figure 2D. For this work, we aimed to achieve the highest surface activation while preserving material topography, thus we utilised borate buffer subsequently as the most appropriate media for this modification.

In the last step, functional polymers were grown via surface initiated-atom transfer radical polymerization (SI-ATRP) from the microparticle surfaces. Activator regenerated by electron transfer (ARGET) ATRP was used to ensure the amounts of copper catalyst could be reduced to low ppm levels, thus lowering any potential cytotoxicity of heavy metal residues in the material after the polymerization. In addition, polymerization conditions were carefully selected to preserve microparticle topography. The high sensitivity of the PLA to the majority of organic solvents made aqueous ATRP the most attractive option and thus a mixture of methanol/water or water only were used as solvents. TPMA was chosen as the metal chelating ligand as it possesses a strong binding affinity towards the catalyst and its complexes show significant stability under these conditions with minimal disproportionation.[47-48] The ligand to catalyst ratio was fixed at 5:1 ratio as it has also been reported that an excess ligand helps to maintain the active catalyst species and protects it from destabilizing side reactions.[49] Reactions were carried out at room temperature using ascorbic acid as the reducing agent at a ratio of 80:1 to copper.[38]

Under the conditions described above, poly(ethylene glycol) methacrylate (PEGMA500) and N-(3-aminopropyl) methacrylamide (APMA) were successfully polymerized from the microparticle

surfaces. To evaluate if a layer of these polymers was effectively coating the microparticles, the chemical compositions of the surfaces after polymerization were analyzed by XPS and ToF-SIMS. In the XPS analysis, wide scan and high resolution spectra of the main components were recorded to obtain complete information of the chemistries present at the outermost layer. Atomic compositions of the microparticles before and after polymerization obtained from the wide scan spectra (see Figure S1, SI) are summarized in Table 1.

Table 1. Atomic compositions obtained from XPS spectra of microparticles (MPs) before and after polymer grafting.

		C at% (285.0 eV)	O at% (532.7 eV)	N at% (399.7 eV)	Br at% (70.1 eV)
Unmodified MPs		59.9	40.1	-	-
Aminolysed MPs		65.7	33.9	0.4	-
BiBB -functionalized MPs		68.4	30.4	0.5	0.7
pPEGMA-grafted MPs	Smooth	71.1	28.4	0.5	0.0
	Dimpled	71.5	28.3	0.1	0.1
pAPMAm-grafted MPs	Smooth	71.2	27.0	1.2	0.6
	Dimpled	73.4	24.6	1.4	0.6

Before functionalization the carbon and oxygen surface concentration for untreated PLA microparticles were detected at concentrations of 59.9 % for C 1s and 40.1 % for O 1s which correlated well with theoretical values for pure PLA of 60 % and 40 % respectively. In addition, peak fitting of the core-level C 1s spectra revealed three main peaks of the same intensity corresponding to each of the three different carbons, confirming the presence of lactic acid units (Figure S1, SI). The peak at the lowest binding energy situated at 285.0 eV was assigned to C-H, the peak at 287.0 eV assigned to C-O-C(=O) and the peak at 289.1 eV assigned to the ester carbon (O-C=O). After reacting with ethylenediamine, the newly appearing N 1s peak (399.7 eV) confirmed successful introduction of amine functionality at the

surface. Although of low intensity, (0.4 % of the total signals), it was possible to resolve two different components. The peak appearing at 399.6 eV was associated with the free amino groups (-C-NH_2) and a second peak at 401.4 eV corresponded to the amide bonds (O=C-NH), with a ratio close to 1:1 confirming covalent linkage of the ethylenediamine, rather than physisorption. Similarly, characteristic ions of these functionalities could be identified in the ToF-SIMS at m/z 26 and m/z 42 corresponding to CN^- and CNO^- negative ions respectively (Figure 4). Using the diagnostic ion CN^- as reference, ToF-SIMS spectra were reconstructed as images and used to illustrate key fragment distributions across the sample. All the microparticles displayed a similar intensity of the CN^- ion confirming a homogeneous modification over the microparticle surfaces (Figure 4B). After the BiBB coupling reaction, a characteristic Br 3d photo electron peak appeared, arising from the covalently bonded bromine at 70.3 eV binding energy (0.7 %) (Figure S1).. In addition, diagnostic signals at m/z 79 and m/z 81 assigned to $^{79}Br^-$ and $^{81}Br^-$ negative ions respectively, were clearly apparent in the ToF-SIMS spectra. A minor component at 67.7 eV (14%) was also observed in the XPS spectrum, which has been previously attributed to physically adsorbed bromine[50-51] and in our case, most likely resulting from HBr generated during this reaction. To visualize the modification, ToF-SIMS images were reconstructed from the Br^- ion intensity map (Figure 3B).

Following growth of polyPEGMA500 brushes from the ATRP initiator modified surfaces, a prominent new peak at 286.5 eV was observed in the C1s core level, corresponding to the C-O bonds of the PEG side chain of the PEGMA500 units (Figure S1). High resolution O 1s spectra also displayed characteristic signals from the pPEGMA layer. Before polymer grafting, untreated PLA microparticles showed two peaks of identical intensity from the two types of oxygens belonging to the ester group, O-C=O at 532.3 eV and O-C=O at 533.9 eV (Figure S1). In contrast, pPEGMA500-grafted MPs exhibited a substantial increase in the intensity of the peak at the lowest binding energy due to the presence of the C-O/C-OH peak from the PEG side chain at 532.7 eV. Moreover, no signal from nitrogen or bromine

could be detected after the polymerization indicating a depth of polymer coverage on the surface which was greater than the penetration depth of the X-ray photoelectrons.

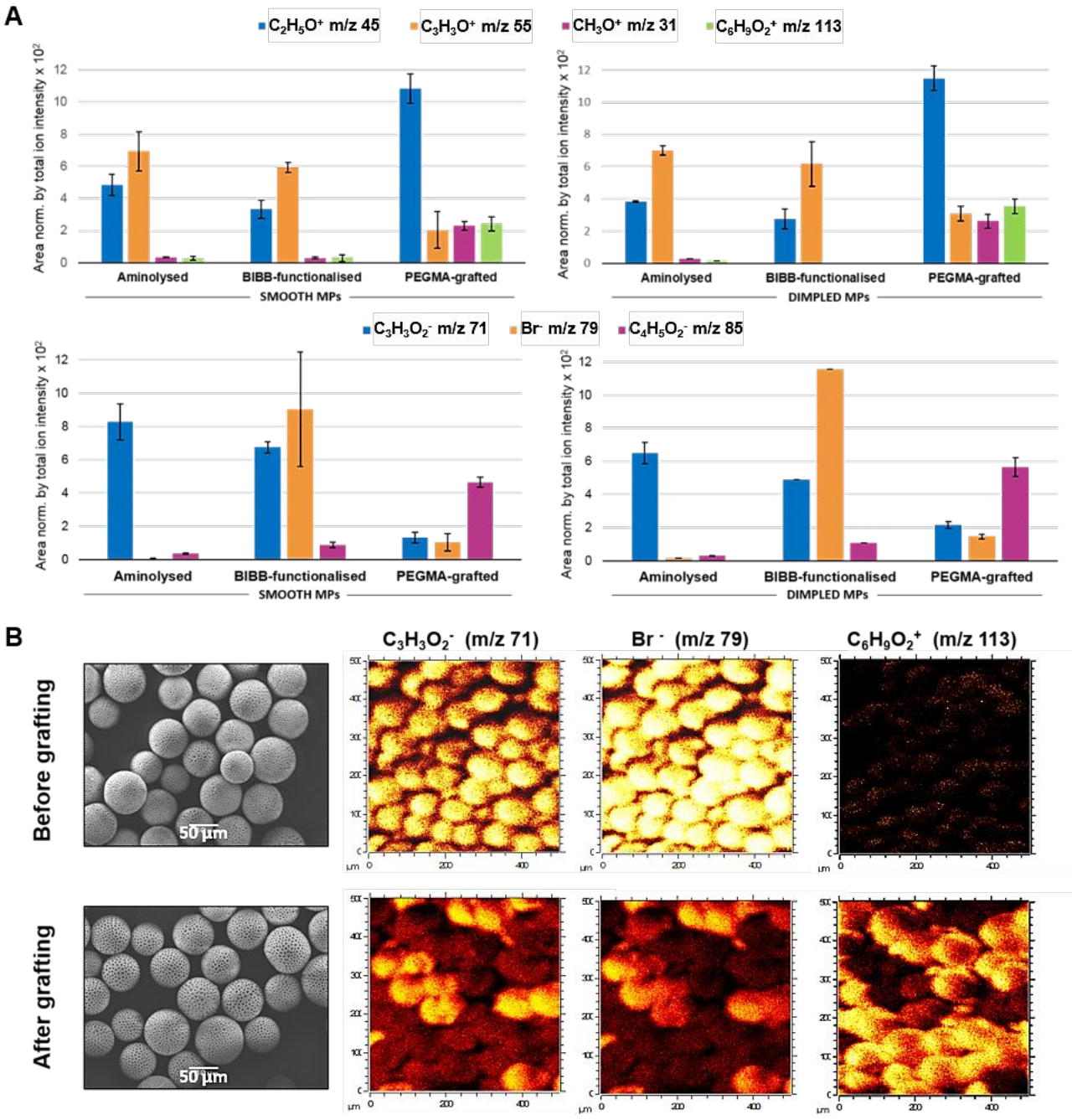

Figure 3. (A) ToF-SIMS ion intensity of smooth (n=3) and dimpled microparticles (n≥2) after aminolysis, BiBB -coupling and PEGMA500 grafting from MPs. Error bars represented as standard deviation of the mean. (B) SEM micrographs of dimpled microparticles and ToF-SIMS images of PLA,

BiBB and PEGMA characteristic ions before and after PEGMA grafting from microparticle surfaces. Scale bars in SEM images = 50μm.

Analyses of the ToF-SIMS data were in good agreement with XPS findings. Characteristic ions from both PLA and PEGMA were identified in the negative and positive ion extraction modes. The most representative PLA ions such as $C_2H_5O^+$ (m/z 45) and $C_3H_3O^+$ (m/z 55) in the positive ionization mode and $C_3H_3O_2^-$ (m/z 71) in the negative mode, and the Br^- ion (m/z 79) from the initiator were used as reference to distinguish surface functionality from the bulk material. Representative ions for PEGMA at m/z 31, 45 (common with PLA) and 113 in the positive mode corresponding to CH_3O^+, $C_2H_5O^+$, $C_6H_9O_2^+$ respectively, and m/z 85 in the negative mode assigned to $C_4H_5O_2^-$ were used to confirm the presence of the PEGMA repeat units. As can be seen in Figure 3A, the intensity of all the PLA and α-bromoisobutyramide-related ions greatly decreased on the pPEGMA-grafted MPs after the polymerizations, as compared to the non-grafted microparticles. Concurrently, the most relevant ions for PEGMA functionality became apparent, as a consequence of the polymethacrylate coating covering the PLA bulk material. In particular, peaks m/z 71 and 79, from PLA and initiator, respectively, and peak m/z 113 from PEGMA unit were used for image reconstruction (Figure 3B). Similar observations to those mentioned above are also reflected in the TOF-SIMS images as demonstrated by a generalized reduction in the ion intensity at m/z 71 and 79, and a consistent presence of ion m/z 113 all over the sample. However, in some cases, a fraction of the pPEGMA-grafted microparticles exhibited lower characteristic ion intensities, indicative of inhomogeneous grafting. We attribute this to insufficient wetting of some of the microparticles during the surface grafting process and consequent lack of contact with reactive monomers for those microparticles retained at the solution/air interface.

To demonstrate that polyPEGMA brushes were growing by a surface-initiated ATRP process, and not due to PEGMA self-polymerization in solution and subsequent adsorption on the surface, grafting

polymerizations were also carried out with the α-bromoisobutyramide -functionalized microparticles in the absence of the catalytic system. Spectra of these samples displayed the same features as those of the microparticles prior to modification (data not shown), confirming that polymer brushes were covalently bonded rather than adsorbed following surface-initiated reactions.

The second monomer chosen for the functionalization of topographical PLA microparticles via aqueous ARGET-ATRP was (3-aminopropyl)methacrylamide (APMA). Monomers containing functional moieties such as primary amines are of value as they provide anchors points for post-polymerization reactions to generate high functional-group density materials for a variety of applications. However, polymerization of monomers bearing primary amine nucleophiles can be particularly challenging via ATRP. This is because accessible amine groups can participate in side-reactions with the halide situated at the chain-ends of the growing polymer and furthermore, can compete in formation of the complexes between ligand and metal catalyst which control the polymerization.[52] For this reason, many prior reports include use of protecting group chemistries to avoid monomer amine-ligand interactions, but these have the disadvantage of requiring a de-protection step to liberate the desired amine after-polymerization. In order to overcome this problem, we used an excess of TPMA, ligand and catalyst and carried out a pre-mixing stage before addition to the monomer. As demonstrated by the first order kinetics obtained from the polymerizations in solution (Figure S2, SI), these methods were found to be suitable for controlled polymerizations of PEGMA and APMA.

The compositions of the surfaces of pAPMA-grafted microparticles after reaction were analyzed by XPS and ToF-SIMS and compared with those of the non-modified microparticles as previously carried out for PEGMA-grafted MPs. Data analysis from both techniques revealed successful grafting of this functionality on smooth and dimpled microparticles. The C 1s core-level spectrum of the grafted-microparticles displayed 2 new peaks at binding energies 286.0 eV and 287.7 eV (Figure S1, SI). These peaks, attributed to the –N-C=O and –C-NH_2/-C-N-(C=O) respectively, accounted for 3 and 10% of the

total atomic composition of the sample. Similarly, and very close to the –O-C=O peak in the O 1s spectrum, a new shoulder was visible at low binding energies (231.2 eV). This signal could be fitted into a peak equally integrating 3% of the total intensity, assigned to the -N-C=O amides of the polyAPMA. Additionally, the nitrogen content in the surface significantly increased from 0.4 % to 1.2 % further confirming the introduction of more amine-functionality because of incorporation of APMA polymer brushes on the microparticles surface.

In agreement with the XPS data, similar observations were found in the ToF-SIMS analysis. As before, $C_3H_3O^+$ (m/z 55), $C_3H_3O_2^-$ (m/z 71) and Br- (m/z 79) were selected as PLA and α-bromoisobutyramide representative ions. However, no specific ions for APMA functionality could be identified in this case as all its characteristic ions match with those already present in the aminolyzed-microparticles. Therefore, only variations in their intensity could be expected. The CH_4N^+ ion (m/z 30) in the positive mode and ions CN^- (m/z 26) and CNO^- (m/z 42) in the negative mode, i.e. typical ions for nitrogen-containing compounds, were used to characterize the polyAPMA microparticles. As can be seen in Figure 4A, reductions in the intensity of the PLA ions were notable for both smooth and dimpled grafted MPs. However, there was not such a clear reduction in Br- ion observed after polymerization, most likely due to counter-ion formation with protonated APMA amine side-chains. The intensity of the three APMA-associated ions under investigation (CH_4N^+, CN^- and CNO^-) significantly increased in the APMA-grafted microparticles when compared to their corresponding intensity before grafting. ToF-SIMS images reconstructed from ions $C_3H_3O_2^-$, $Br^-$and CN^- also illustrate these results (Figure 4B). Although PLA and BiBB ions remained visually almost the same before and after polymerization, with no substantial variations in their intensity, an evident increase in the presence of CN^- ions across the sample was perceived.

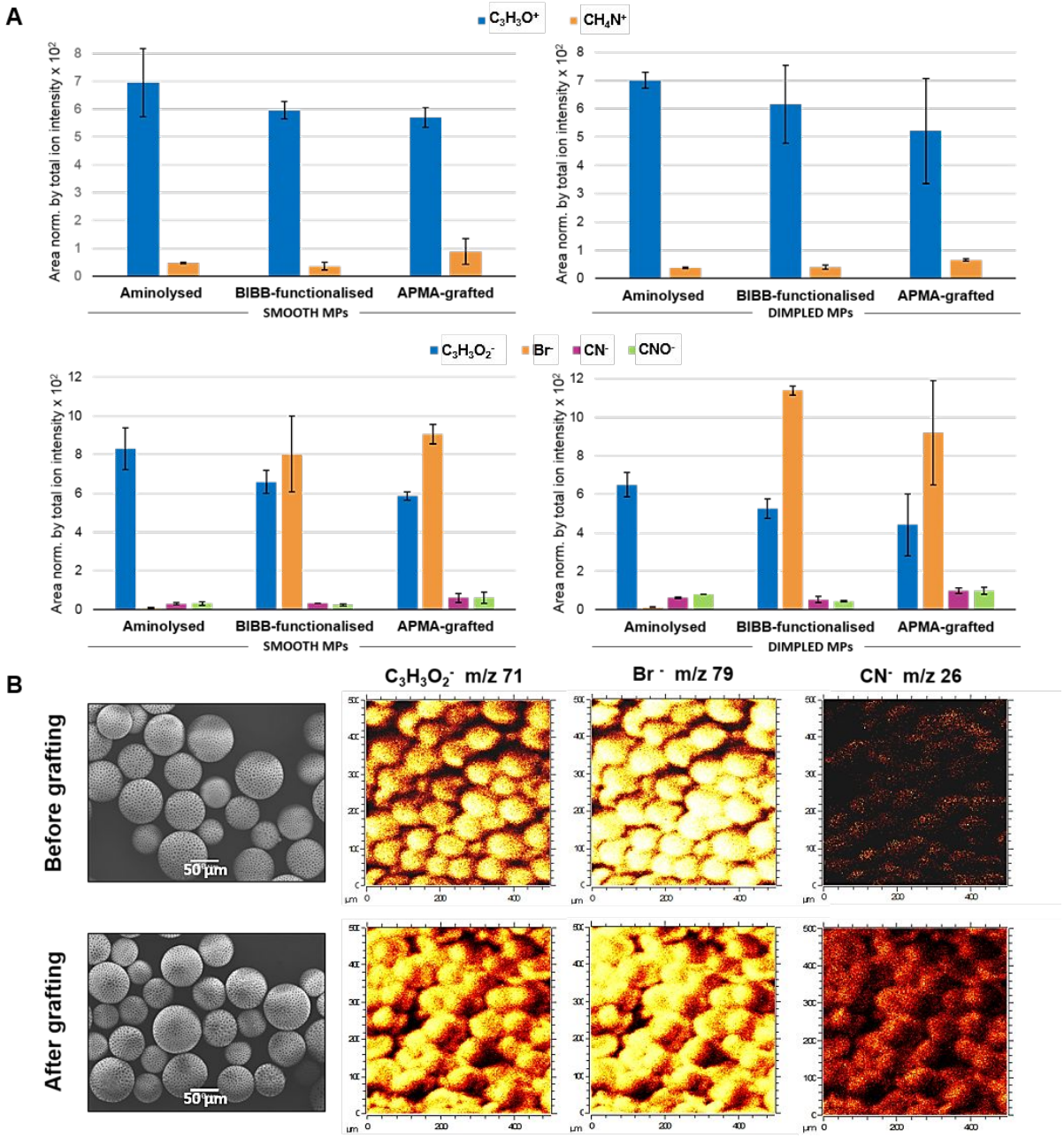

Figure 4. (A) ToF-SIMS ion intensity of smooth (n=3) and dimpled microparticles (n≥2) after aminolysis, BiBB -coupling and APMA grafting from MPs. Error bars represented as standard deviation of the mean. (B) SEM micrographs of dimpled microparticles and ToF-SIMS images of PLA, BiBB and APMA characteristic ions before and after APMA grafting from microparticle surface. Scale bars in SEM images = 50µm.

Surface analysis performed on APMA-grafted microparticles revealed the presence of the polymer layer on the MPs. However, signals confirming this modification were not as intense as those obtained for PEGMA-coated MPs, implying that a reduced coverage of the surface was obtained, or that thinner polymer brush layers were synthesized. However, the microparticles did not aggregate during the polymerization, suggesting retention of charge stabilization after pAPMA grafting, and the final grafted microparticles maintained good integrity of the particle topography after reaction, as can be appreciated in the SEM images (Figure 4B).

Three-dimensional cell aggregate *in vitro* culture platforms have been particularly useful for both large-scale expansion and lineage-specific differentiation of stem cells.[53-56] Use of microparticles offers more tunable cell culture systems with increased control over cell phenotype and fate for scalable cell culture with high surface area-to-volume ratios.[57] Several studies have demonstrated the individual effects of surface chemistry[58-59] and varied topographical features[25, 60] on cell phenotype, but more limited investigations into the combined effects of both.[22] This study therefore aimed to use these chemically functionalized textured microparticles to investigate further the relative importance of topography and surface chemistry on mammalian cell adhesion and formation of cell-microparticle aggregates in 3D co-cultures. By varying both topography and surface chemistry on microparticles independently, surfaces with the same chemical modification but different topographies or, alternatively, surfaces with various chemical modifications but the same topographical features could be compared with respect to their ability to support mammalian cells in 3D cultures. Subsequent experiments evaluated the interactions of microparticles with the four different surface chemistries, i.e. PLA, aminolysed-PLA, pPEGMA-PLA and pAPMA-PLA, and the two topographies (smooth and dimpled) in the culture and expansion of hiMSCs.

As shown in Figure 5, hiMSCs attached readily to the microparticles when co-cultured, with pAPMA-PLA dimpled microparticles showing a significantly higher cell attachment relative to the untreated dimpled microparticles. However, there were no other statistically significant differences between microparticles of different topographies, but with the same surface chemistry, in relation to cell attachment (Figure 5A). Importantly, cell proliferation was maintained for ten days on all the surfaces (Figure 5B). This indicated their suitability for extended cell culture, although there were no differences again between smooth and dimpled microparticles of the same chemistry in supporting cell expansion. By day 10, there was a negligible difference between cell proliferation between the untreated and surface functionalised PLA microparticles. We postulate that this is because the cells have proliferated to a point where they have most probably covered all the surfaces available for attachment and have secreted their own extracellular matrix, decreasing the effects of surface chemistry at that time point. High cell viability was observed across all samples, as assessed by the Live/Dead Viability/Cytotoxicity assay, with larger aggregates observed using APMA-PLA microparticles (Figure 5C).

To investigate the interplay of surface chemistry and topography in materials for cell aggregate co-culture applications, cell aggregation was investigated 6 hours post-seeding of hiMSCs on the various microparticles. With pPEGMA-treated microparticles, cells preferred to form cell-cell aggregates rather than cell-microparticle aggregates. Furthermore, more evident cell-microparticle aggregation was observed with pAPMA-functionalized microparticles of both topographies under investigation (Figure 5D).

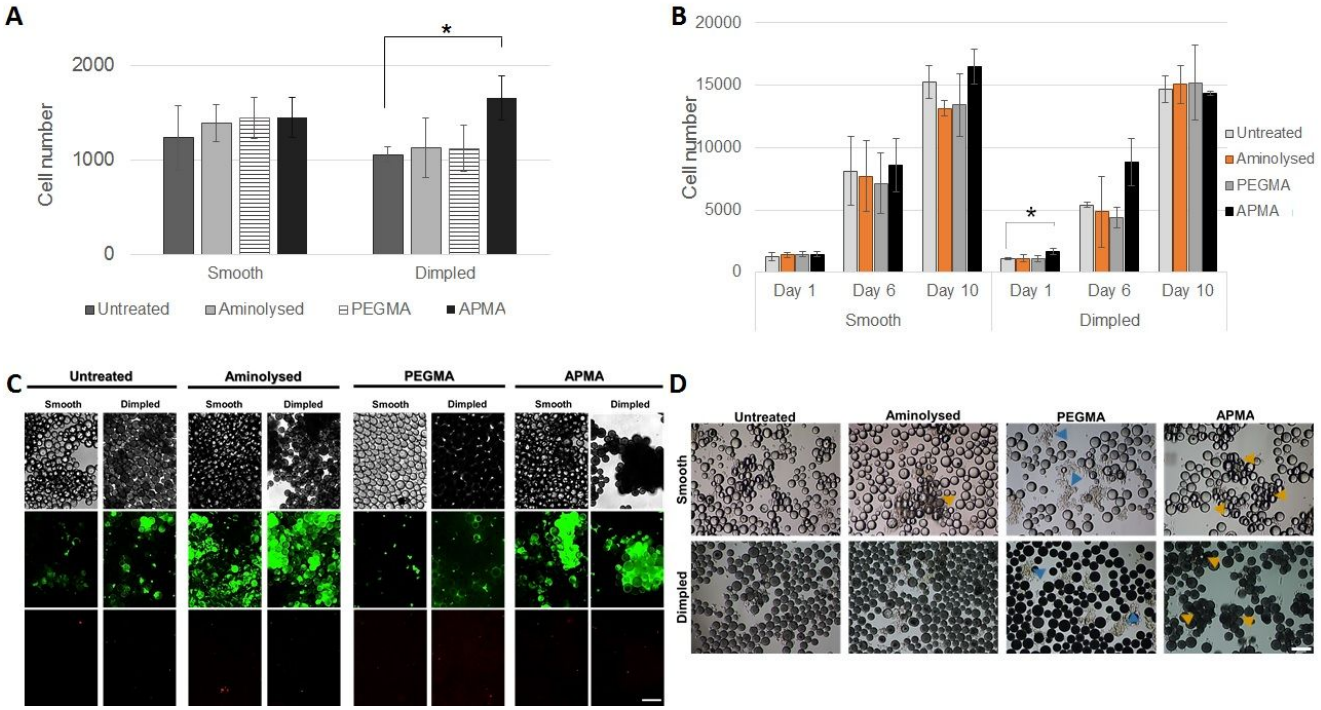

Figure 5. (A) hiMSC attachment, assessed using PrestoBlue™, 24 hours post-seeding (n=3; ANOVA; *p<0.05). (B) Proliferation of hiMSCs on chemically modified textured microparticles over 10 days, assessed using PrestoBlue™ (n=3; ANOVA; *p<0.05). (C) Representative fluorescence microscopy images of Live-Dead staining of hiMSCs cultured on unfunctionalized and chemically modified microparticles 48 hours post-seeding (green= calcein-stained; red= ethidium bromide-stained). (D) Representative images of aggregates beginning to form 6 hours post-seeding of hiMSCs on untreated and chemically modified textured microparticles. With pPEGMA-treated microparticles, cells preferred to form cell aggregates (blue arrowheads) rather than cell-microparticle aggregates (yellow arrowheads) as found with other untreated and modified microparticles. (Scale bars = 100μm).

Further evaluation of the interactions between the microparticles and the hiMSCs was carried out via automated image analysis (CellProfiler[61]). Supplementary Figure 3A shows the CellProfiler pipeline used to identify cell aggregates and generate quantitative metrics, with the quantified data shown in Figure 6. Figures 6A and 6B indicates that the largest cell-containing aggregates were formed with the

positively charged particles (pAPMA-PLA). Once more, there were no significant differences between smooth and dimpled particles of the same surface chemistry. Within a given topography, cell aggregate size was influenced by the surface chemistry of the microparticles and was greatest on the most positively charged surfaces, pAPMA-PLA, irrespective of the surface topography. This is in line with previous studies, which suggest that surface chemistry is the determining factor in cell adhesion.[14, 62-63]

In relation to the numbers of aggregates formed (Figure 6C and 6D), there were variations across the set of microparticles. In terms of topography, there was a significantly lower number of aggregates formed when hiMSCs were seeded on unmodified dimpled PLA microparticles relative to the smooth unmodified microparticles. This result is again consistent with previous studies that have reported that substrates with non-oriented topographies exhibited lower cell adhesion,[64] albeit for surfaces of different charges then the PLA-based microparticles in this study.

In these assays, aggregates could be formed from both cell-particle associations and cell-cell interactions. Thus, when considering the relative sizes of the particles (~50μm in diameter) and the cells (~20μm), it is likely that particle-cell aggregates would be larger than cell-cell aggregates, accounting for the fact that the positively charged particles formed the largest aggregates with the cells. However, in cases of reduced particle-cell association, more cell-cell aggregates could form, thus the total numbers of aggregates observed did not correlate directly with the chemistry/topography that yielded the largest agglomerates. Accordingly, it is important to consider cell behavior, not simply cell-surface attachment, when evaluating materials for culture, expansion or application of particular cell types.

The results suggest that size and number of hiMSC aggregates formed is primarily influenced by surface chemistry of the incorporated microparticles. This aligns with previous findings by Le Saux *et al*., wherein sizes of topographical features on non-flat silicon surfaces were found to influence the number of adherent endothelial cells to a limited extent, while the density of the adhesion ligand RGD governed much more strongly the degree of cell spreading and engagement of cell surface receptors.[62]

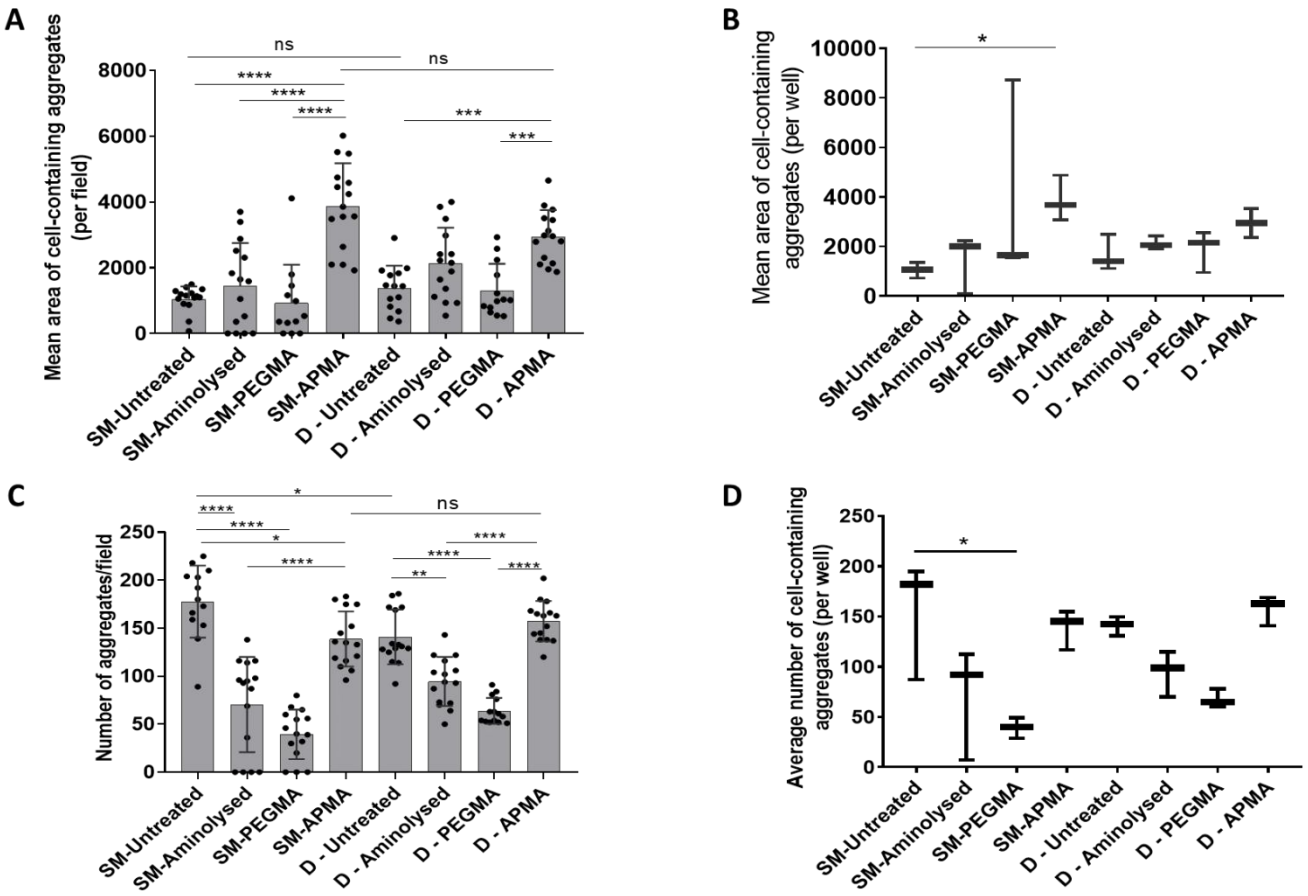

Figure 6. (A) Mean areas of cell-containing aggregates (per field of view) 6 hours post-seeding of hiMSCs on chemically modified textured microparticles (ANOVA). (B) Box-and-whiskers plot of mean areas of cell-containing aggregates (per well) 6 hours post-seeding of hiMSCs on chemically modified textured microparticles (Kruskal-Wallis post-hoc test). (C) Average numbers of hiMSC-containing aggregates (per field of view) 6 hours post-seeding of hiMSCs on microparticles. (D) Box-and-whiskers plot of average numbers of cell-containing aggregates (per well) 6 hours post-seeding of hiMSCs on microparticles. (SM: Smooth; D: dimpled; *p<0.05 **p<0.01, ***p<0.001, ****p<0.0001).

We therefore embarked on a functional cell assay to explore how aminoethyl (following aminolysis), pPEGMA and pAPMA modifications to the surfaces of microparticles affected the behavior

of hiPSC-CMs. Attachment of hiPSC-CMs across all microparticle conditions was evident 24hrs post-seeding (Figure 7). It was observed that hiPSC-CMs formed cell-cell aggregates more readily in the presence of the untreated and pPEGMA-treated microparticles, i.e. those particles expected to be slightly negatively charged under the experimental conditions. In contrast, hiPSC-CM-microparticle aggregates formed to the greatest extent with the aminolysed and pAPMA-treated microparticles, which were positively charged (Figure 7A). These data were corroborated by quantifying sizes and numbers of hiPSC-CMs microparticle aggregates (methods and supplementary figure 3B) by field and by well (Figure 7B and 7C). Aggregates were significantly smaller for pPEGMA treated microparticles than the other surfaces, as expected based on the known anti-attachment properties for PEG-based materials when chain-extended.[36] Aminolysed and pAPMA treated microparticles formed the largest cell-microparticle aggregates, again in line with expectations based on surface charge (Figure 7B). Quantification of the numbers of hiPSC-CM--microparticle aggregates showed that the number of cell-microparticle aggregates was significantly higher for pAPMA treated microparticles compared to the other three surfaces (Figure 7C), likely attributable to the higher charge density of these microparticles from the extended charged pAPMA brushes.

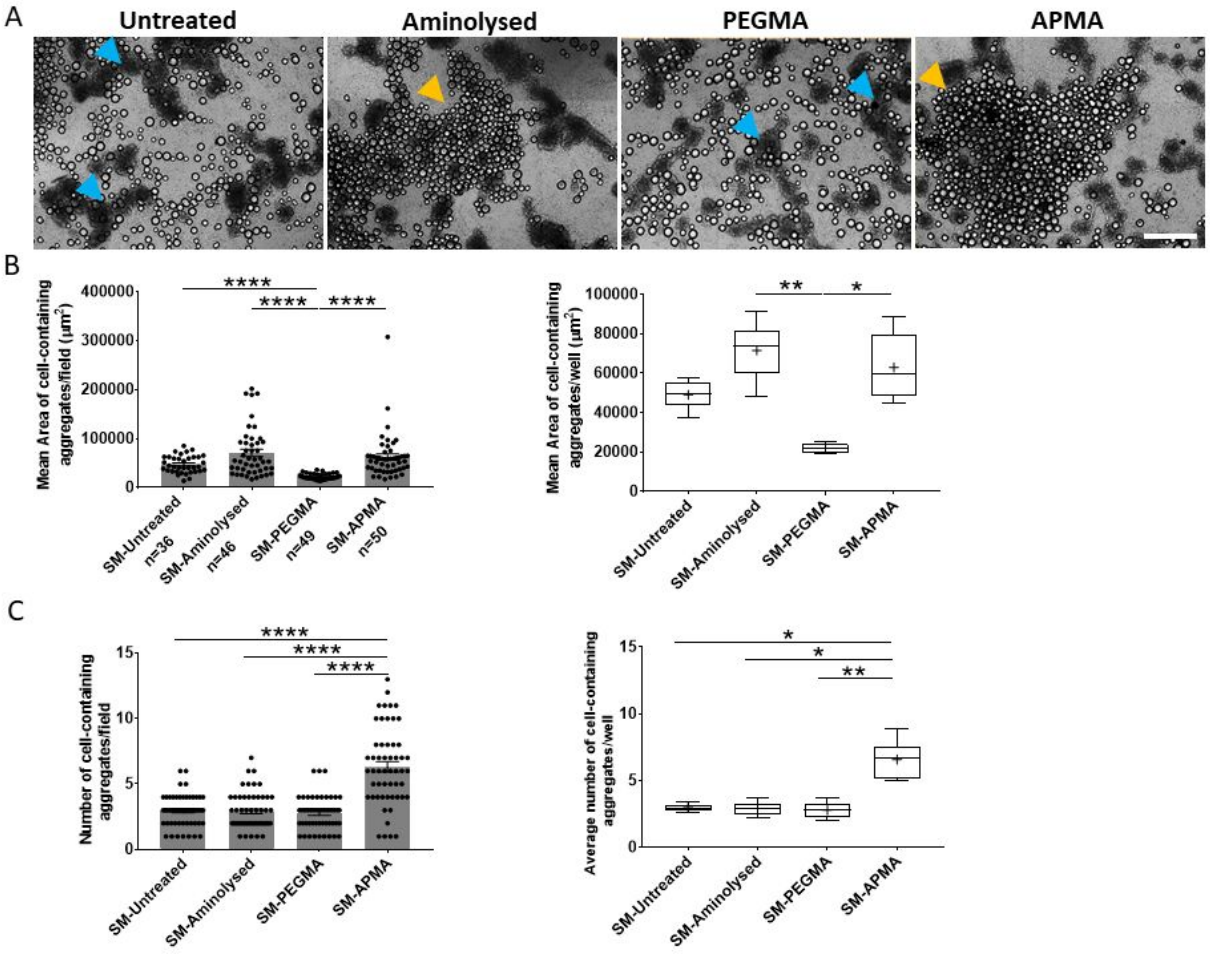

Figure 7. (A) Representative images of spontaneously contracting hiPSC-CM-microparticle aggregates formed 24hrs after seeding on smooth untreated and chemically-modified microparticles. Cell aggregates (marked with blue arrows) and cell-microparticle aggregates (marked with yellow arrows) were preferred in untreated/pPEGMA and aminolysed/pAPMA modified microparticles respectively (scale bar represents 500µm). (B) Mean areas of cell-microparticle aggregates formed 24hrs post-seeding of hiPSC-CMs on smooth (SM) untreated and chemically-modified microparticles plotted as scatter dot bar plot (where each scatter dot represents a field of view, bars represent mean values and error bars ± SEM) and box-and-whiskers plot (+ denotes mean values; n=6 wells).(C) Numbers of cell-microparticle aggregates formed 24hrs post-seeding of hiPSC-CMs untreated and chemically-modified microparticles plotted as scatter dot bar plot (each scatter dot represents a field of view, bars represent mean values and error bars

± SEM; n=54/condition). Box-and-whiskers plot of average numbers of cell-microparticle aggregates (+ denotes mean values; n=6 wells). One-way ANOVA (Kruskal-Wallis post-hoc) statistical tests performed (*p<0.05, ** p<0.01, *** p<0.001 and **** p<0.0001).

To quantify functional performance across the hiPSC-CM-microparticle aggregates (Figure 8A), an open-source contractility tool, MUSCLEMOTION[42], was used to analyse videos taken at 30 frames / second (Figure 8B). Aminolysed and pAPMA modifications generated hiPSC-CM-particle aggregates with significantly higher contraction amplitude (Figure 8C) and relaxation rates (Figure 8D) relative to those formed from untreated and pPEGMA modified particles. Contraction rate was also significantly increased in aminolysed hiPSC-CM-particle aggregates relative to untreated and pPEGMA modified particles (Figure 8E). These changes in contraction parameters, governed by enhanced electrical stimulation (cardiac action potential properties), are consistent with enhanced functional performance of the hiPSC-CMs.[42, 65-66]

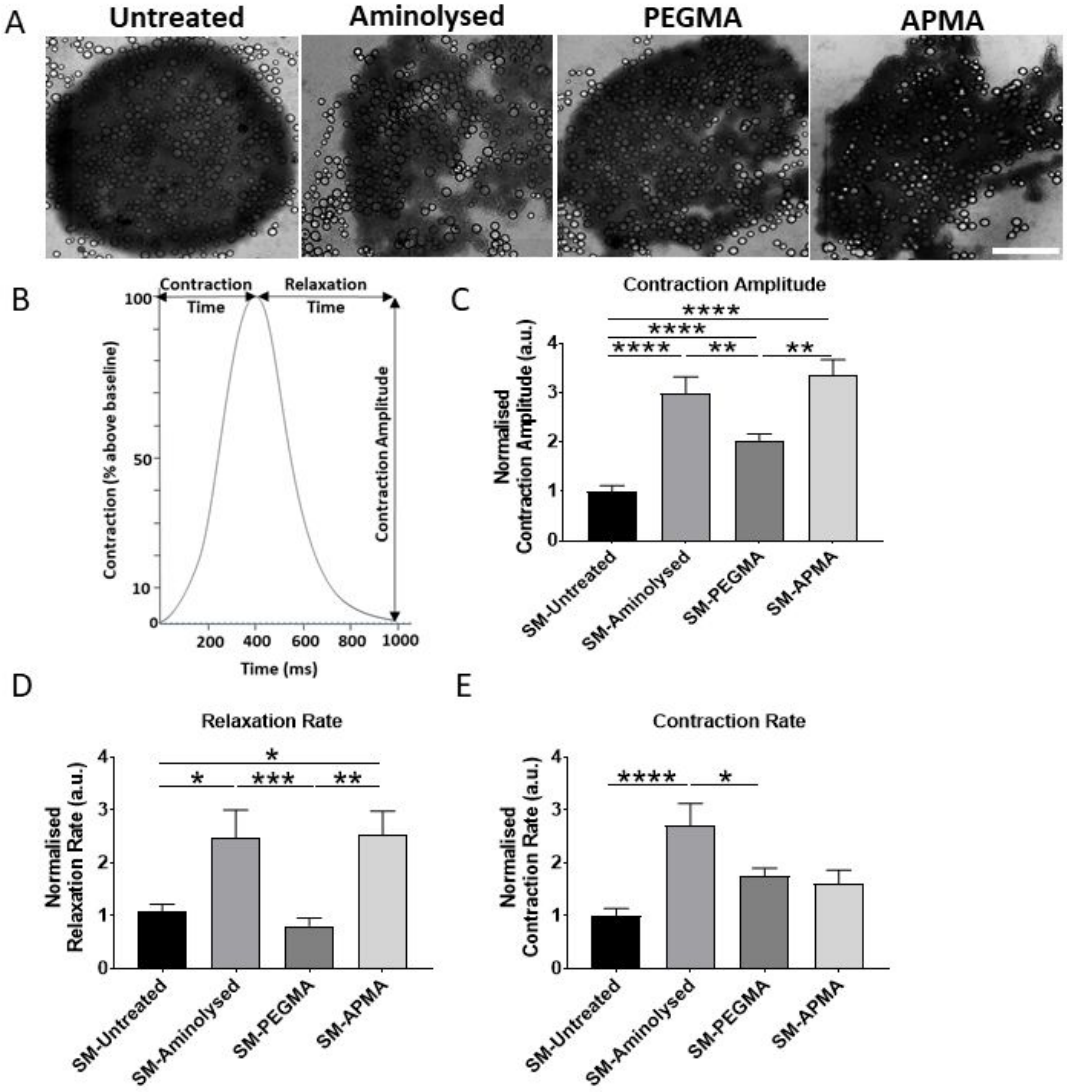

Figure 8. (A) Representative images of spontaneously contracting interconnected hiPSC-CM-microparticle aggregates taken 4 days post-seeding (Scale bar represents 500μm). (B) Schematic shows the parameters measured for contractility analysis. Diagram shows one contraction peak. Contraction time represents the time taken for a peak to reach its maximum amplitude (contraction amplitude (0 (baseline) -100)). Relaxation time is the time taken for a peak to return to baseline (0). (C-E) Contraction parameters were quantified from video images of hiPSC-CM-microparticles aggregates taken 48hrs post-seeding. Images were taken from fields with high cell-microparticle interactions (untreated (n=20), aminolysed (n=23), pPEGMA (n=41) and pAPMA (n=11)). One-way ANOVA statistical tests were performed (*p<0.05, **p<0.01, ***p<0.001 and **** p<0.0001). Parameters represented as bar plots (±SEM). Contraction parameters for hiPSC-CM-microparticle aggregates of chemically modified

microparticles were normalised to untreated condition: (C) Contraction amplitude; (D) Relaxation rate (contraction amplitude/relaxation time) and (E) Contraction rate (contraction amplitude/contraction time).

These data together indicated that functional materials useful for long-term co-culture in mammalian stem cell aggregates could be generated from cytocompatible polyester microparticles, and confirmed the complex interplay of topography and surface chemistry in engineering cell-microparticle aggregates. The results also highlighted the importance of functional group chemistry for improving biological function at cell-material interfaces, in this instance exemplified by contractile activity in cardiomyocytes.

Conclusions

In this study, we have introduced a novel strategy for surface functionalization of biodegradable PLA microparticles with varying surface chemistries and topologies. The method was demonstrated to be compatible with topographical features presented on the substrates, revealing a new route to obtain topo-chemical combinations on polyester-based biomaterials. These materials were found to be useful for long-term 3D co-culture with mammalian cells, and a sub-set of the microparticles were supportive of cell attachment, growth and cardiomyocyte contraction. The data also confirmed the complexities in delineating effects of topography and functional group chemistry in controlling cell-material interactions, with the dominant effect in our assays arising from microparticles which displayed polymeric positive charges. The functionalities identified in ToF-SIMS confirmed that amine groups from the initial aminolysis reactions to derivatise the PLGA, and from subsequent grafting of poly(N-(3-Aminopropyl) methacrylamide hydrochloride) were present in the surfaces which showed the most efficacy in retaining stem cell phenotype and cardiomyocyte attachment and resultant function. These data sets thus verified

the utility of surface-mapping microparticles by ToF-SIMS and correlation of surface properties with biological interaction. The results overall highlighted the need for fine control in synthesis to generate functionally- and topographically well-defined biomaterials, and the need to modulate these parameters for key application areas of cell- microparticle aggregates, such as tissue engineering and *ex vivo* culture applications.

Associated content

XPS spectra, polymerization kinetics and a schematic of the analysis script used to quantify REBL-PAT-CM microparticle aggregates are provided in Supporting Information.

Author information

Corresponding authors

* Cameron Alexander (Cameron.alexander@nottingham.ac.uk) and Felicity Rose (Felicity.rose@nottingham.ac.uk).

Author contributions

‡These authors contributed equally. All authors have given approval to the final version of the manuscript.

Funding sources

This work was supported by the Engineering and Physical Sciences Research Council [grant numbers EP/N006615/1 and EP/K005138/1, EP/N03371X/1]; and the Royal Society [Wolfson Research Merit Award WM150086] (to CA), National Centre for the Replacement, Refinement & Reduction of Animals in Research [grant numbers CRACK-IT:35911-259146, NC/K000225/1]; the British Heart Foundation [grant numbers SP/15/9/31605, RG/15/6/31436, PG/14/59/31000, RG/14/1/30588, P47352/CRM].

Acknowledgments

We thank the Nanoscale and Microscale Research Centre and Dr Emily Smith at University of Nottingham for providing access to SEM and XPS instrumentation, and the SLIM facility and Dr Tim Self, School of Life Sciences, University of Nottingham for advanced microscopy. We also thank Christine Grainger-Boultby and Dr Jiang Long for instrumental support and technical assistance, and Professors Kevin Shakesheff (School of Pharmacy, University of Nottingham) for helpful discussions.

Data Access Statement

All raw data created during this research are openly available from the corresponding authors (felicity.rose@nottingham.ac.uk, cameron.alexander@nottingham.ac.uk) and at the University of Nottingham Research Data Management Repository (https://rdmc.nottingham.ac.uk/) and all analyzed data supporting this study are provided in the SI accompanying this paper.

References

1. Danhier, F.; Ansorena, E.; Silva, J. M.; Coco, R.; Le Breton, A.; Préat, V. PLGA-Based Nanoparticles: An Overview of Biomedical Applications. *J. Controlled Release* **2012,** *161*, 505-522.
2. Tyler, B.; Gullotti, D.; Mangraviti, A.; Utsuki, T.; Brem, H. Polylactic Acid (PLA) Controlled Delivery Carriers for Biomedical Applications. *Adv. Drug Delivery Rev.* **2016,** *107*, 163-175.
3. Gao, X.; Song, J. L.; Zhang, Y. C.; Xu, X.; Zhang, S. Q.; Ji, P.; Wei, S. C. Bioinspired Design of Polycaprolactone Composite Nanofibers as Artificial Bone Extracellular Matrix for Bone Regeneration Application. *ACS Appl. Mater. Interfaces* **2016,** *8*, 27594-27610.
4. Casey, L. M.; Pearson, R. M.; Hughes, K. R.; Liu, J. M. H.; Rose, J. A.; North, M. G.; Wang, L. Z.; Lei, M.; Miller, S. D.; Shea, L. D. Conjugation of Transforming Growth Factor Beta to Antigen-Loaded Poly(Lactide-Co-Glycolide) Nanoparticles Enhances Efficiency of Antigen-Specific Tolerance. *Bioconjugate Chem.* **2018,** *29*, 813-823.
5. Gossmann, R.; Fahrlander, E.; Hummel, M.; Mulac, D.; Brockmeyer, J.; Langer, K. Comparative Examination of Adsorption of Serum Proteins on HSA- and PLGA-Based Nanoparticles Using Sds-Page and Lc-Ms. *Eur. J. Pharm. Biopharm.* **2015,** *93*, 80-87.
6. van Oss, C. J. Long-Range and Short-Range Mechanisms of Hydrophobic Attraction and Hydrophilic Repulsion in Specific and Aspecific Interactions. *J. Mol. Recognit.* **2003,** *16*, 177-190.
7. Jeong, J. H.; Lim, D. W.; Han, D. K.; Park, T. G. Synthesis, Characterization and Protein Adsorption Behaviors of Plga/Peg Di-Block Co-Polymer Blend Films. *Colloids Surf., B* **2000,** *18*, 371-379.
8. Barry, J. J. A.; Silva, M.; Shakesheff, K. M.; Howdle, S. M.; Alexander, M. R. Using Plasma Deposits to Promote Cell Population of the Porous Interior of Three-Dimensional Poly(D,L-Lactic Acid) Tissue-Engineering Scaffolds. *Adv. Funct. Mater.* **2005,** *15*, 1134-1140.
9. Quirk, R. A.; Briggs, D.; Davies, M. C.; Tendler, S. J. B.; Shakesheff, K. M. Characterization of the Spatial Distributions of Entrapped Polymers Following the Surface Engineering of Poly(Lactic Acid). *Surf. Interface Anal.* **2001,** *31*, 46.
10. Duque-Sanchez, L.; Brack, N.; Postma, A.; Pigram, P. J.; Meagher, L. Optimisation of Grafting of Low Fouling Polymers from Three-Dimensional Scaffolds Via Surface-Initiated Cu(0) Mediated Polymerisation. *J. Mater. Chem. B* **2018,** *6*, 5896-5909.

11. Sun, Y.; Xing, Z.; Xue, Y.; Mustafa, K.; Finne-Wistrand, A.; Albertsson, A.-C. Surfactant as a Critical Factor When Tuning the Hydrophilicity in Three-Dimensional Polyester-Based Scaffolds: Impact of Hydrophilicity on Their Mechanical Properties and the Cellular Response of Human Osteoblast-Like Cells. *Biomacromolecules* **2014,** *15*, 1259-1268.
12. Nugroho, R. W. N.; Pettersson, T.; Odelius, K.; Hoglund, A.; Albertsson, A. C. Force Interactions of Nonagglomerating Polylactide Particles Obtained through Covalent Surface Grafting with Hydrophilic Polymers. *Langmuir* **2013,** *29*, 8873-8881.
13. Santander-Borrego, M.; Chirila, T. V.; Shadforth, A. M. A.; Whittaker, A. K.; Blakey, I. Effect of Changes in the Surface Chemistry and Topography of Poly(2-Hydroxyethyl Methacrylate) on the *in Vitro* Attachment of Human Corneal Epithelial Cells. *J. Bioact. Compat. Polym.* **2018,** *33*, 321-331.
14. Joy, A.; Cohen, D. M.; Luk, A.; Anim-Danso, E.; Chen, C.; Kohn, J. Control of Surface Chemistry, Substrate Stiffness, and Cell Function in a Novel Terpolymer Methacrylate Library. *Langmuir* **2011,** *27*, 1891-1899.
15. Lilge, I.; Schonherr, H. Control of Cell Attachment and Spreading on Poly(Acrylamide) Brushes with Varied Grafting Density. *Langmuir* **2016,** *32*, 838-847.
16. Privalova, A.; Markvicheva, E.; Sevrin, C.; Drozdova, M.; Kottgen, C.; Gilbert, B.; Ortiz, M.; Grandfils, C. Biodegradable Polyester-Based Microcarriers with Modified Surface Tailored for Tissue Engineering. *J. Biomed. Mater. Res., Part A* **2015,** *103*, 939-948.
17. Satomi, T.; Nagasaki, Y.; Kobayashi, H.; Otsuka, H.; Kataoka, K. Density Control of Poly(Ethylene Glycol) Layer to Regulate Cellular Attachment. *Langmuir* **2007,** *23*, 6698-6703.
18. Luo, J.; Zhang, H.; Zhu, J.; Cui, X.; Gao, J.; Wang, X.; Xiong, J. 3-D Mineralized Silk Fibroin/Polycaprolactone Composite Scaffold Modified with Polyglutamate Conjugated with BMP-2 Peptide for Bone Tissue Engineering. *Colloids Surf., B* **2018,** *163*, 369-378.
19. Rianna, C.; Radmacher, M. Influence of Microenvironment Topography and Stiffness on the Mechanics and Motility of Normal and Cancer Renal Cells. *Nanoscale* **2017,** *9*, 11222-11230.
20. Peng, L.; Zhou, S. L.; Yang, B.; Bao, M. M.; Chen, G. J.; Zhang, X. H. Chemically Modified Surface Having a Dual-Structured Hierarchical Topography for Controlled Cell Growth. *ACS Appl. Mater. Interfaces* **2017,** *9*, 24339-24347.
21. Sangsanoh, P.; Israsena, N.; Suwantong, O.; Supaphol, P. Effect of the Surface Topography and Chemistry of Poly(3-Hydroxybutyrate) Substrates on Cellular Behavior of the Murine Neuroblastoma Neuro-2a Cell Line. *Polym. Bull.* **2017,** *74*, 4101-4118.
22. Macgregor, M.; Williams, R.; Downes, J.; Bachhuka, A.; Vasilev, K. The Role of Controlled Surface Topography and Chemistry on Mouse Embryonic Stem Cell Attachment, Growth and Self-Renewal. *Materials* **2017,** *10*, 1081.
23. Chen, Z. T.; Bachhuka, A.; Han, S. W.; Wei, F.; Lu, S.; Visalakshan, R. M.; Vasilev, K.; Xiao, Y. Tuning Chemistry and Topography of Nanoengineered Surfaces to Manipulate Immune Response for Bone Regeneration Applications. *ACS Nano* **2017,** *11*, 4494-4506.
24. Li, Q.; Zhang, B.; Kasoju, N.; Ma, J.; Yang, A.; Cui, Z.; Wang, H.; Ye, H. Differential and Interactive Effects of Substrate Topography and Chemistry on Human Mesenchymal Stem Cell Gene Expression. *Int. J. Mol. Sci.* **2018,** *19*, 2344.
25. Unadkat, H. V.; Hulsman, M.; Cornelissen, K.; Papenburg, B. J.; Truckenmüller, R. K.; Carpenter, A. E.; Wessling, M.; Post, G. F.; Uetz, M.; Reinders, M. J. T.; Stamatialis, D.; van Blitterswijk, C. A.; de Boer, J. An Algorithm-Based Topographical Biomaterials Library to Instruct Cell Fate. In *Proc Natl Acad Sci U S A*, **2011**, pp 16565-16570.
26. Lee, J. H.; Lee, C.-S.; Cho, K. Y. Enhanced Cell Adhesion to the Dimpled Surfaces of Golf-Ball-Shaped Microparticles. *ACS Appl. Mater. Interfaces* **2014,** *6*, 16493-16497.
27. Bartneck, M.; Schulte, V. A.; Paul, N. E.; Diez, M.; Lensen, M. C.; Zwadlo-Klarwasser, G. Induction of Specific Macrophage Subtypes by Defined Micro-Patterned Structures. *Acta Biomater* **2010,** *6*, 3864-3872.
28. Solanki, A.; Shah, S.; Memoli, K. A.; Park, S. Y.; Hong, S.; Lee, K. B. Controlling Differentiation of Neural Stem Cells Using Extracellular Matrix Protein Patterns. *Small* **2010,** *6*, 2509-2513.
29. Berry, C. C.; Campbell, G.; Spadiccino, A.; Robertson, M.; Curtis, A. S. G. The Influence of Microscale Topography on Fibroblast Attachment and Motility. *Biomaterials* **2004,** *25*, 5781-5788.
30. Charest, J. L.; Eliason, M. T.; Garcia, A. J.; King, W. P. Combined Microscale Mechanical Topography and Chemical Patterns on Polymer Cell Culture Substrates. *Biomaterials* **2006,** *27*, 2487-2494.
31. Cousins, B. G.; Zekonyte, J.; Doherty, P. J.; Garvey, M. J.; Williams, R. L. Manufacturing a Nanometre Scale Surface Topography with Varying Surface Chemistry to Assess the Combined Effect on Cell Behaviour. *Int. J. Nano Biomater.* **2008**, *1*, 320-338
32. Motornov, M.; Sheparovych, R.; Katz, E.; Minko, S. Chemical Gating with Nanostructured Responsive Polymer Brushes: Mixed Brush Versus Homopolymer Brush. *ACS Nano* **2008,** *2*, 41-52.
33. Santiago, L. Y.; Nowak, R. W.; Peter Rubin, J.; Marra, K. G. Peptide-Surface Modification of Poly(Caprolactone) with Laminin-Derived Sequences for Adipose-Derived Stem Cell Applications. *Biomaterials* **2006,** *27*, 2962-2969.
34. Uhlig, K.; Wischerhoff, E.; Lutz, J.-F.; Laschewsky, A.; Jaeger, M. S.; Lankenau, A.; Duschl, C. Monitoring Cell Detachment on Peg-Based Thermoresponsive Surfaces Using Tirf Microscopy. *Soft Matter* **2010,** *6*, 4262-4267.
35. Hucknall, A.; Rangarajan, S.; Chilkoti, A. In Pursuit of Zero: Polymer Brushes That Resist the Adsorption of Proteins. *Advanced Materials* **2009,** *21*, 2441-2446.
36. Saeed, A.; Francini, N.; White, L.; Dixon, J.; Gould, T.; Rashidi, H.; Al Ghanami, R. C.; Hruschka, V.; Redl, H.; Saunders, B. R.; Alexander, C.; Shakesheff, K. M. A Thermoresponsive and Magnetic Colloid for 3D Cell Expansion and Reconfiguration. *Advanced Materials* **2015,** *27*, 662-668.

37. Gilchrist, S. E.; Rickard, D. L.; Letchford, K.; Needham, D.; Burt, H. M. Phase Separation Behavior of Fusidic Acid and Rifampicin in PLGA Microspheres. *Mol. Pharmaceutics* **2012,** *9*, 1489-1501.
38. Paterson, S. M.; Brown, D. H.; Chirila, T. V.; Keen, I.; Whittaker, A. K.; Baker, M. V. The Synthesis of Water-Soluble Phema Via ARGET ATRP in Protic Media. *J. Polym. Sci., Part A: Polym. Chem.* **2010,** *48*, 4084-4092.
39. Mori, T.; Kiyono, T.; Imabayashi, H.; Takeda, Y.; Tsuchiya, K.; Miyoshi, S.; Makino, H.; Matsumoto, K.; Saito, H.; Ogawa, S.; Sakamoto, M.; Hata, J.; Umezawa, A. Combination of hTERT and bmi-1, E6, or E7 Induces Prolongation of the Life Span of Bone Marrow Stromal Cells from an Elderly Donor without Affecting Their Neurogenic Potential. *Mol. Cell. Biol*. **2005**, *25*, 5183-5195.
40. Lamprecht, M. R.; Sabatini, D. M.; Carpenter, A. E. Cellprofiler: Free, Versatile Software for Automated Biological Image Analysis. *Biotechniques* **2007,** *42*, 71-75.
41. Mosqueira, D.; Mannhardt, I.; Bhagwan, J. R.; Lis-Slimak, K.; Katili, P.; Scott, E.; Hassan, M.; Prondzynski, M.; Harmer, S. C.; Tinker, A.; Smith, G. W.; Carrier, L.; Williams, P. M.; Gaffney, D.; Eschenhagen, T.; Hansen, A.; Denning, C. Crispr/Cas9 Gene Editing in Human Pluripotent Stem Cell-Cardiomyocytes Provides a Platform for Modeling Hypertrophic Cardiomyopathy. *Hum. Gene Ther.* **2018,** *29*, A93-A94.
42. Sala, L.; van Meer, B. J.; Tertoolen, L. G. J.; Bakkers, J.; Bellin, M.; Davis, R. P.; Denning, C.; Dieben, M. A. E.; Eschenhagen, T.; Giacomelli, E.; Grandela, C.; Hansen, A.; Holman, E. R.; Jongbloed, M. R. M.; Kamel, S. M.; Koopman, C. D.; Lachaud, Q.; Mannhardt, I.; Mol, M. P. H.; Mosqueira, D.; Orlova, V. V.; Passier, R.; Ribeiro, M. C.; Saleem, U.; Smith, G. L.; Burton, F. L.; Mummery, C. L. Musclemotion: A Versatile Open Software Tool to Quantify Cardiomyocyte and Cardiac Muscle Contraction *in Vitro* and *in Vivo*. *Circ Res* **2018,** *122*, e5-e16.
43. Motulsky, H. J.; Brown, R. E. Detecting Outliers When Fitting Data with Nonlinear Regression - a New Method Based on Robust Nonlinear Regression and the False Discovery Rate. *BMC Bioinf.* **2006,** *7*, 123.
44. Croll, T. I.; O'Connor, A. J.; Stevens, G. W.; Cooper-White, J. J. Controllable Surface Modification of Poly(Lactic-Co-Glycolic Acid) (Plga) by Hydrolysis or Aminolysis I: Physical, Chemical, and Theoretical Aspects. *Biomacromolecules* **2004,** *5*, 463-473.
45. Gyarmati, B.; Hegyesi, N.; Pukanszky, B.; Szilagyi, A. A Colourimetric Method for the Determination of the Degree of Chemical Cross-Linking in Aspartic Acid-Based Polymer Gels. *eXPRESS Polym. Lett.* **2015,** *9*, 154-164.
46. Svobodova, J.; Rypacek, F. Polyglutamate Copolymers as a Tissue-Engineering Platform: Polymer Scaffold Modification Through Aminolysis of Poly(Gamma-Benzyl-L-Glutamate-Co-2,2,2-Gamma-Trichlorethyl-L-Glutamate). *Eur. Polym. J.* **2012,** *48*, 183-190.
47. Tsarevsky, N. V.; Braunecker, W. A.; Matyjaszewski, K. Electron Transfer Reactions Relevant to Atom Transfer Radical Polymerization. *J. Organomet. Chem.* **2007,** *692*, 3212-3222.
48. Fantin, M.; Isse, A. A.; Gennaro, A.; Matyjaszewski, K. Understanding the Fundamentals of Aqueous ATRP and Defining Conditions for Better Control. *Macromolecules* **2015,** *48*, 6862-6875.
49. Simakova, A.; Averick, S. E.; Konkolewicz, D.; Matyjaszewski, K. Aqueous Arget Atrp. *Macromolecules* **2012,** *45*, 6371-6379.
50. Chua, C. K.; Pumera, M. Renewal of Sp(2) Bonds in Graphene Oxides Via Dehydrobromination. *J. Mater. Chem.* **2012,** *22*, 23227-23231.
51. Alexander, M. R.; Whittle, J. D.; Barton, D.; Short, R. D. Plasma Polymer Chemical Gradients for Evaluation of Surface Reactivity: Epoxide Reaction with Carboxylic Acid Surface Groups. *J. Mater. Chem.* **2004,** *14*, 408-412.
52. Mendonca, P. V.; Averick, S. E.; Konkolewicz, D.; Serra, A. C.; Popov, A. V.; Guliashvili, T.; Matyjaszewski, K.; Coelho, J. F. J. Straightforward Arget Atrp for the Synthesis of Primary Amine Polymethacrylate with Improved Chain-End Functionality under Mild Reaction Conditions. *Macromolecules* **2014,** *47*, 4615-4621.
53. Sart, S.; Tsai, A. C.; Li, Y.; Ma, T. Three-Dimensional Aggregates of Mesenchymal Stem Cells: Cellular Mechanisms, Biological Properties, and Applications. *Tissue Eng., Part B* **2014,** *20*, 365-380.
54. Ahrens, C. C.; Dong, Z. Y.; Li, W. Engineering Cell Aggregates through Incorporated Polymeric Microparticles. *Acta Biomater.* **2017,** *62*, 64-81.
55. Abecasis, B.; Aguiar, T.; Arnault, E.; Costa, R.; Gomes-Alves, P.; Aspegren, A.; Serra, M.; Alves, P. M. Expansion of 3D Human Induced Pluripotent Stem Cell Aggregates in Bioreactors: Bioprocess Intensification and Scaling-up Approaches. *J Biotechnol* **2017,** *246*, 81-93.
56. Giacomelli, E.; Bellin, M.; Sala, L.; van Meer, B. J.; Tertoolen, L. G. J.; Orlova, V. V.; Mummery, C. L. Three-Dimensional Cardiac Microtissues Composed of Cardiomyocytes and Endothelial Cells Co-Differentiated from Human Pluripotent Stem Cells. *Development*, **2017**, pp 1008-1017.
57. Bratt-Leal, A. M.; Carpenedo, R. L.; Ungrin, M.; Zandstra, P. W.; McDevitt, T. C. Incorporation of Biomaterials in Multicellular Aggregates Modulates Pluripotent Stem Cell Differentiation. *Biomaterials* **2011,** *32*, 48-56.
58. Patel, A. K.; Celiz, A. D.; Rajamohan, D.; Anderson, D. G.; Langer, R.; Davies, M. C.; Alexander, M. R.; Denning, C. A Defined Synthetic Substrate for Serum-Free Culture of Human Stem Cell Derived Cardiomyocytes with Improved Functional Maturity Identified Using Combinatorial Materials Microarrays. *Biomaterials* **2015,** *61*, 257-265.
59. Shao, W.; He, J.; Sang, F.; Ding, B.; Chen, L.; Cui, S.; Li, K.; Han, Q.; Tan, W. Coaxial Electrospun Aligned Tussah Silk Fibroin Nanostructured Fiber Scaffolds Embedded with Hydroxyapatite-Tussah Silk Fibroin Nanoparticles for Bone Tissue Engineering. *Mater Sci Eng C Mater Biol Appl* **2016,** *58*, 342-351.

60. Abadi, P. P. S. S.; Garbern, J. C.; Behzadi, S.; Hill, M. J.; Tresback, J. S.; Heydari, T.; Ejtehadi, M. R.; Ahmed, N.; Copley, E.; Aghaverdi, H.; Lee, R. T.; Farokhzad, O. C.; Mahmoudi, M. Engineering of Mature Human Induced Pluripotent Stem Cell-Derived Cardiomyocytes Using Substrates with Multiscale Topography. *Adv. Funct. Mater.* **2018,** *28*, 1707378.
61. Carpenter, A. E.; Jones, T. R.; Lamprecht, M. R.; Clarke, C.; Kang, I. H.; Friman, O.; Guertin, D. A.; Chang, J. H.; Lindquist, R. A.; Moffat, J.; Golland, P.; Sabatini, D. M. CellProfiler: Image Analysis Software for Identifying and Quantifying Cell Phenotypes. *Genome Biol.* **2006,** *7,* R100.
62. Le Saux, G.; Magenau, A.; Boecking, T.; Gaus, K.; Gooding, J. J. The Relative Importance of Topography and RGD Ligand Density for Endothelial Cell Adhesion. *PLoS One* **2011,** *6*, e21869.
63. Anselme, K.; Ploux, L.; Ponche, A. Cell/Material Interfaces: Influence of Surface Chemistry and Surface Topography on Cell Adhesion. *J. Adhes. Sci. Technol.* **2010,** *24*, 831-852.
64. Meredith, D. O.; Eschbach, L.; Riehle, M. O.; Curtis, A. S. G.; Richards, R. G. Microtopography of Metal Surfaces Influence Fibroblast Growth by Modifying Cell Shape, Cytoskeleton, and Adhesion. *J. Orthop. Res.* **2007,** *25*, 1523-1533.
65. Ribeiro, M. C.; Tertoolen, L. G.; Guadix, J. A.; Bellin, M.; Kosmidis, G.; D'Aniello, C.; Monshouwer-Kloots, J.; Goumans, M. J.; Wang, Y. L.; Feinberg, A. W.; Mummery, C. L.; Passier, R. Functional Maturation of Human Pluripotent Stem Cell Derived Cardiomyocytes *in Vitro*-Correlation between Contraction Force and Electrophysiology. *Biomaterials* **2015,** *51*, 138-150.
66. Blazeski, A.; Zhu, R.; Hunter, D. W.; Weinberg, S. H.; Zambidis, E. T.; Tung, L. Cardiomyocytes Derived from Human Induced Pluripotent Stem Cells as Models for Normal and Diseased Cardiac Electrophysiology and Contractility. *Prog Biophys Mol Biol* **2012,** *110*, 166-177.

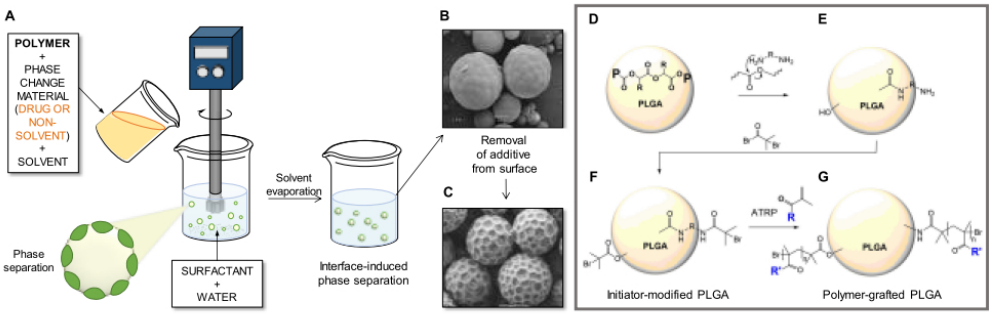

TOC graphic

82x45mm (300 x 300 DPI)